Methods used in *Klimaatlas*, the Danish Climate Atlas

DMI Report 24-11

June 2024

The Danish Meteorological Institute

Title	Methods used in *Klimaatlas*, the Danish Climate Atlas
Author	National Center for Klimaforskning (NCKF) at DMI
Editor	Peter Thejll
Institution	Danish Meteorological Institute
Language	English
Keywords	Climate, Bias correction, Extreme value analysis, sea level, extreme precipitation, storm surge.

Contents

Changes in this version

Current version v2024a, June 2024

This version introduces a new indicators related to fire, dry periods and meterological drought. In addition, several existing precipitation indicators have been moved into a new "tørke" (drought) group. The new groupings and indicators (with their corresponding IDs) are:

- Fire danger (*brandfare*)

    - Average fire danger across years / seasons
    - Number of days with "very high" fire danger
    - Number of days with "extreme" fire danger

- Drought (tørke)

    - Number of dry days (moved from *Nedbør* (precipitation) group) (108)
    - Longest dry period (moved from *Nedbør* (precipitation) group) (109)
    - Number of years / season that are "dry" (110)
    - Number of periods of minimum five consecutive dry days (112)
    - Number of periods of minimum ten consecutive dry days

The number of ensemble members has been expanded from 65 to 72.

Klimaatlas data is now archived in the Zenodo archive. As a result, klimaatlas data and reports now have a Digital Object Identifier (DOI) associated with them. This version of Klimaatlas can therefore be referenced as:
Danish Meteorological Institute. (2024). DMI Klimaatlas v2024a - Projections of climate indicators over Denmark [Data set]. Zenodo. `https://doi.org/10.5281/zenodo.11402836`

Previous versions of Klimaatlas data have also be archived retrospectively. The full archive can be found at: `https://zenodo.org/communities/klimaatlas`

Excel spreadsheets have been converted to a new format that is intended to be both human-readable and machine readible. The medium emissions scenario (RCP4,5 / SSP2-4,5) were added to the Kommune reports, together with overview "cartoon-strips" showing changes under different emissions scenarios.

Version v2022a, February 2023.

In this update of the climate atlas, we added (1) the low emission climate scenario RCP2.6, (2) sea level projections from the latest IPCC report, and (3) additional climate model data for

the RCP4.5 and RCP8.5 scenarios.

Regarding (1) and (3), the list of models used in the current data set can be found in Tables 7 and 8.

Regarding (2), we updated the mean sea level data regionalized from IPCC AR6, which means it is now based on the new generation of emission scenarios, "Shared Socioeconomic Pathways" (SSPs). The scenarios used in this report for sea level rise assessment are SSP1-2.6/RCP2.6, SSP2-4.5/RCP4.5 and SSP5-8.5/RCP8.5. As something new, our uncertainty estimates now include the expert judgement of potential contributions from melting ice sheets not well-captured by the climate models; often called low confidence processes, as part of "deep uncertainty" related to sea level rise. The inclusion of this estimate from the latest IPCC report results in a larger uncertainty interval, especially through an increased 90-percentile of the high-emission scenario RCP8.5.

Improved calculation methods have given rise to minor changes with this update. Among the atmospheric indices, we change the order of statistical processing and interpolation for some of the indices, with only small changes discernible in the mean. We have added an updated flow-chart of the processing used for the atlas, on page 30. Looking at the change in median values expressed as a percentage of the width of the old confidence interval from the 10 to the 90 percentile, we note some changes, mainly of minor sizes. Indices of wind and extreme precipitation show the most pronounced local changes.

With the method update, it appears that the older versions of the *Klimaatlas* underestimated the widths of confidence intervals for indexes related to extremes, compared to the present version of the *Klimaatlas*. Hence, these have increased - again - especially for extreme precipitation and winds.

Lastly, while the regional climate model projections of the SSP-scenarios are still being prepared by the international research community, we have added a first assessment of the new generation of global climate model projections (CMIP6, based on the SSP-scenarios) over Northern Europe and how they compare to the previous projections (CMIP5, based on RCP-scenarios). The assessment can be found in subsection (Section 5.1.1), with more details in the report Christiansen [2022].

The previous versions of this report had the DMI numbers 19-17, 20-18, 20-20 and 21-41 and are still downloadable at the links

```
https://www.dmi.dk/fileadmin/Rapporter/2021/DMI_Rep-21-41.pdf
https://www.dmi.dk/fileadmin/Rapporter/2020/DMI_SR_20_20.pdf
https://www.dmi.dk/fileadmin/Rapporter/2020/DMI_SR_20_18.pdf
```

Version v2021a, December 2021.

In this version we release high resolution time series for 8 variables, namely - tas, tasmin, tasmax, pr, sfcWind, sfcWindmax, rsds, potevap, which are used to produce a range of indexes in the *Klimaatlas*. These time-series are released at a 1x1 km grid as daily values, and are made available as netcdf files for download by the users.

Users of these expert-only data should be aware that the files are large and download times long. Use of the *wget* solution is recommended.
We have changed the algorithm for calculating indexes 008 and 009 (i.e. heat-wave days and warm-wave days) and now release corrected versions of these indexes in the *Klimaatlas*, which are consistent with the calculations applied to DMI's climatological data. This means that both data and figures are updated. Compared to the updated numbers, the previous method resulted in too many days being counted by several in the mean, and up to 12 days in some models.

We introduced a new bias-adjustment method of handling (low) extremes which influenced, to a small degree, indexes 301, 302, 401 and 402. New values for these were calculated and are part of version 2021a release. The change had to do with ensuring that small negative values are not produced during the bias-adjustment.

Two new sea level and storm surge indicators: frequency and accumulated duration of sea level exceeding current local warning level. The 10.000 year storm surge events are still subject to research, and an update is underway – read section 6.1.2 for details. We have changed the unit of the frequency of 20-year storm surge events to number of events per 20 year period.

The present data release, version 2021a, is identical to version v2020b, except for the indices 008, 009, 301, 302, 401 and 402 and the ocean information indexes 210, 211 and 212, which are updated.

Section 4 of the older versions of this report has been shortened and edited for clarity and the text therein now only details the procedures actually applied—see, e.g. version 20-20, for the older material.

Version v2020b, December 2020

With the update to version 2020b in December 2020, *Klimaatlas* has been expanded with 19 new indicators. The new data presents more details on the future changes in temperature, winds, evaporation, sunshine, frequent and rare storm surges.

Fourteen new atmospheric indicators: Daily high and low temperatures, maximum and minimum temperatures, annual and diurnal temperature intervals, heatwaves (hedebølger og varmebølger), frost days, growing season length, mean wind speed, number of storm events, potential evaporation, and solar radiation.

Five new sea level and storm surge indicators: 100- and 10,000-year storm surge events, 1- and 5-year sea level events, and the change in frequency of current 20-year storm surge events.

The complete overview of the indicators in the current version of *Klimaatlas* can be found in Table 2.

The main updates to text concern calculation of new temperature indices (in Section 8) and the data for rare storm surge events (in Section 5).

The previous version of this report had the DMI number 20-20 and is still available at the DMI index of all reports:
`https://www.dmi.dk/fileadmin/Rapporter/2020/DMI_SR_20_20.pdf`.

Version v2020a, June 2020

The previous version of this report had the DMI number 20-18 and is still available at the DMI index of all reports:
`https://www.dmi.dk/fileadmin/Rapporter/2020/DMI_SR_20_18.pdf`.

Changes compared to version 1.1 / v2019a:
With version v2020a, *Klimaatlas* has been updated to include 8 new indicators: the mean number of dry days, the mean duration for the longest dry period, and 5, 20, and 50 year events for hourly and daily precipitation. Furthermore, *Klimaatlas* is now based on data from more climate models; up to 57 models for daily values and 35 models for hourly values. Data for sea level and storm surges is unchanged since v2019a.

Note that some index numbers have changed since the previous version: the indices for 2, 10, and 100-year events for hourly precipitation are now 151, 153, and 156 (previously 108,

109, and 110), and the indices for 2, 10, and 100-year events for 24-hour precipitation are now 157, 159, and 162 (previously 111, 112, and 113).

Version v2019a, October 2019

This older version of this report had the DMI number 19-17 and is still available at the DMI index of all reports:

`https://www.dmi.dk/fileadmin/Rapporter/2019/DMIrapport_19_17.pdf.`

1   Introduction

The Danish National Climate Atlas, *Klimaatlas*, provides Danish society with relevant and easy-to-use information on expected future changes in climate, including changes in atmospheric temperatures, precipitation and derived indices, as well as from the sea surrounding Denmark (sea-level and storm surges).

The information is based on observational data and models of the expected climate of the future, derived from the EURO-CORDEX archives [Jacob et al., 2014], (`https://euro-cordex.net/`). Such model data are, when taken raw, not expected to correspond closely to reality but must be adjusted or calibrated so that they become more realistic. In this report we describe the applied calibration method together with other processing applied.

Klimaatlas is available online at

`http://www.dmi.dk/klimaatlas`

and is accompanied with detailed help and user-information. During the planning and calculation period leading up to the release of the *Klimaatlas* in 2019, thorough reviews of the literature on climate model calibration were carried out, and extensive testing of methods performed. In particular, inter-comparison of methods were performed so that the best methods could be chosen for use in *Klimaatlas*.

It is **the purpose of this Technical Report** to give the necessary details for the methods chosen, and the tests and comparisons that lie behind the choices, as well as to give an overview of the full set of processing leading to the results displayed.

Reading Guide: The report is made up of several sections, and reading each in isolation should be possible. In section 1.1 a sort of 'Executive Summary' is given; section 2 introduces methods used in this report to determine how to best perform so-called model-calibration, and introduces important terminology used throughout the report - the discussion of how we chose our methods may not interest all readers; section 3 is analytical and shows how we determined which method to use in calibrating models in the case these are used for *non-extreme* climate properties; section 4 analyses the same problem, but for use in *extremes* of climate change - precipitation events such as cloudbursts, and sea-level; in sections 5 and 6 methods used for producing projections of future sea levels and storm surges are described; in the online version of *Klimaatlas* uncertainties are shown as the 10 and 90 percentiles of the spread due to model choice, in section 7 we discuss issues related to 'uncertainty'; for each climate index provided we describe in detail the implementation in section 8 - if the reader is only interested in how climate indices were calculated in practise, this is the section to read.

1.1   Brief summary of the contents of *Klimaatlas*

Klimaatlas was launched in 2019, updated twice in 2020, and time-series of climate variables were made available in 2021. In 2022 information for RCP2.6 was added.

Scenario description	Atmospheric indexes	Oceanic indexes
High	RCP 8.5	SSP 5-8.5
Medium	RCP 4.5	SSP 2-4.5
Low	RCP 2.6	SSP 1-2.6

Table 1: Emission scenarios used in the *Klimaatlas* version 2024a.

Each index describes absolute values as well as changes in the index, expressed in percent or physical units as appropriate. Information, except the ocean indices, is available on a 1x1 km grid as well as on an aggregated basis for municipalities and main catchment areas. The ocean indices are available on 34 coastal stretches.

Information is provided in several data-formats – **.xlsx** spreadsheets, **.netcdf** files and as 'GIS layers'. These data are intended for users requiring download of material for further processing, but *Klimaatlas* also provides an online display of the information, with documentation and user guides. Information is made available for the four seasons (and an annual value) for multiple emission scenarios (See Table 1). Four time periods are used - a present-day reference period (1981-2010) and three future periods (near future 2011-2040, mid-century 2041-2070, and end of century 2071-2100).

The current list of climate indices in *Klimaatlas* are listed in Table 2.

Table 2: Summary of climate indices,v2024a.

Index number	Name of index	Notes on implementation
001	Mean temperature	Mean temperature in °C over a year or a season.
002	Daily maximum temperature	The mean daily maximum temperature (in °C) seasonally or annually. Describes the highest temperature to be expected on a typical day.
003	Daily minimum temperature	The mean daily minimum temperature (°C) seasonally or annually. Describes the lowest temperature to be expected on a typical day.
004	Maximum temperature	The maximum temperature (°C) in the season/annually, calculated as the mean of the 30 years' occurrences seasonally/annually.
005	Minimum temperature	The minimum temperature (°C) in the season/annually, calculated as the mean of the 30 years' occurrences seasonally/annually.

Table 2: Summary of climate indices,v2024a.

Index number	Name of index	Notes on implementation
006	Annual temperature range	Average annual difference between highest and lowest temperature in °C.
007	Diurnal temperature range	Seasonal/annual average (in °C) of the range between daily maximum and minimum temperatures.
008	Heatwave days	Number of heat-wave days annually. A 'heatwave' is indicated when the average of the maximum temperature, over at least three consecutive days, is above 28 °C, not counting the first two days of each heatwave.
009	Warm-wave days	Number of warm-wave days annually. A 'warm-wave' is indicated when the average of the maximum temperature, over at least three consecutive days, is above 25 °C, not counting the first two days of each warm-wave.
010	Frost days	Number of days seasonally/annually where the lowest temperature is below freezing (0 °C).
011	Growing season length	Number of days between the years' first contiguous 6 days of daily mean temperature above 5 °C to the years last 6-day period of daily mean temperatures above 5 °C.
101	Mean precipitation	Mean precipitation in mm/day across a year or a season.
102	Max daily precipitation	Sum of precipitation during that day of the year or season when maximum 24-hour precipitation-sum was observed.
103	5-day max precipitation	5-day sum of precipitation in that 5-day period of the year or season with largest 5-day sum of precipitation.
104	14-day max precipitation	14-day sum of precipitation in that 14-day period of the year or season with largest 14-day sum of precipitation.

Table 2: Summary of climate indices,v2024a.

Index number	Name of index	Notes on implementation
105	Number of days with over 10 mm precipitation per day.	
106	Number of days with over 20 mm precipitation per day.	
107	Number of cloudbursts per year	Number of days with more than 15 mm precipitation in 30 minutes.
108	Number of dry days	Number of days of the year or season with precipitation below 1 mm.
109	Maximum dry spell length	Length of the longest period of the year or season with consecutive days with precipitation below 1 mm.
110	Fraction of dry seasons	Defined by sum of precipitation more than one standard deviation below the sum for the historical period
112	Number of 5-day dry spells	Number of dry periods of minimum length 5 days with less than 1mm precipitation per day
115	Number of 10-day dry spells	Number of dry periods of minimum length 10 days with less than 1mm precipitation per day
151	2-year event hourly precipitation	Precipitation-sum for one hour that occurs with a return-period of two years.
152	5-year event hourly precipitation	Precipitation-sum for one hour that occurs with a return-period of five years.
153	10-year event hourly precipitation	Precipitation-sum for one hour that occurs with a return-period of ten years.
154	20-year event hourly precipitation	Precipitation-sum for one hour that occurs with a return-period of 20 years.
155	50-year event hourly precipitation	Precipitation-sum for one hour that occurs with a return-period of 50 years.
156	100-year event hourly precipitation	Precipitation-sum for one hour that occurs with a return-period of 100 years.

Table 2: Summary of climate indices,v2024a.

Index number	Name of index	Notes on implementation
157	2-year event in 24-hour precipitation	Precipitation-sum over 24 hours that occurs with a return-period of two years.
158	5-year event 24-hour precipitation	Precipitation-sum over 24 hours that occurs with a return-period of five years.
159	10-year event 24-hour precipitation	Precipitation-sum over 24 hours that occurs with a return-period of 10 years.
160	20-year event 24-hour precipitation	Precipitation-sum over 24 hours that occurs with a return-period of 20 years.
161	50-year event 24-hour precipitation	Precipitation-sum over 24 hours that occurs with a return-period of 50 years.
162	100-year event 24-hour precipitation	Precipitation-sum over 24 hours that occurs with a return-period of 100 years.
201	Mean sea level wrt. coastline	Increase in sea-level, in cm
202	Storm surge 20-year events	Height of storm surge, in cm, of the 20-year event, relative to reference level.
203	Storm surge 50-year event	Height of storm surge, in cm, of the 50-year event, relative to reference level.
204	Storm surge 100-year event	Height of storm surge, in cm, of the 100-year event, relative to reference level.
205	Storm surge 10 000 year event	Height of storm surge, in cm, of the 10 000 year event, relative to reference level.
206	1-year sea level event	Height of the sea level, in cm, of the 1 year event, relative to reference level.
208	5-year sea level event	Height of the sea level, in cm, of the 5-year event, relative to reference level.

Table 2: Summary of climate indices,v2024a.

Index number	Name of index	Notes on implementation
210	Frequency of storm surge 20-year event	Frequency of the storm surge events per 20 years defined relative to current (i.e. historical), reference level.
211	Frequency of storm surge events exceeding current local warning level	Change of the frequency of the storm surge exceeding current local warning level, in number of events per year, relative to reference level.
212	Accumulated duration of sea level exceeding current local warning level	Change of accumulated duration of sea level exceeding current local warning level, in hours per year, relative to reference level.
301	Mean wind speed	Average wind speed (in m/s) over a year or a season.
302	Extreme wind	Number of days in a year or season with a maximum wind speed above 25 m/s.
401	Solar radiation	Seasonal/annual average of the daily sum of the direct and diffuse radiation from the Sun reaching the (horizontal) surface, in W/m^2.
402	Potential evaporation	The seasonal/annual average potential evaporation (in mm/day) that could evaporate, as given by the Makkink formula Jacobs and Bruin [1998]
501	Mean Fire Weather Index	Mean FWI across seasons and year
502	Days with very high fire risk	Number of days with fire weather index above 18.5
503	Days with extremely high fire risk	Number of days with fire weather index above 29.5

2   Method overview

Model calibration essentially deals with the reality that distributions of climate model data are not usually identical to distributions of the same quantities observed. The differences

can lie in different mean values, or, usually, in distributions that neither have the same mean nor the same shape (widths, for instance). Methods that deal with the task of making model data distributions more or less similar to observed data, are here generally termed "calibration" methods, with additional nomenclature to indicate precisely which form of adjustment is used. These concepts will be discussed below.

Calibration methods can be quite different, as we shall see, based on which variable considered. Common to them all is that they are based on somehow using information taken from the observational world. An issue arises if the observational data are not very extensive, so each method may have to be adapted to the particulars of the situation.

In climate-change work a 'reference period' is often employed, such as 1986-2005 in IPCC AR5 and 1995-2014 in IPCC AR6, as a baseline to calculate climate change. The beginning and length of this period are typically carefully chosen in order to achieve a number of things. One goal is to help diminish the influence the effect of natural variability – i.e. the reference period should be long enough to smooth out variations, but not so long it extends over important phases of climate change. We have here chosen as 'reference period' 1981-2010 which is a compromise to have a period as close to present as possible, 30 years long, and to symmetrically overlap the AR5 reference period.

A 'calibration period' is also chosen, which is the period during which observed and model data both exist. The calibration period is used to determine the data transformations required. This period may be different for different climate variables due to observational constraints.

As is the norm in climate work, statements about future expected climate change are often made in terms of the change between two periods – one will then typically be the reference period while the other is some 'future period' such as 2011-2040, 2041-2070, and 2071-2100 (these will be used in *Klimaatlas*, see Figure 2). For example, precipitation-change is quantified in terms of a ratio, while for temperature it is given as a difference.

In this work we shall see two calibration methods evaluated and used. These will be discussed in detail below, but are, in general, the "Bias Correction" methods that transform model data by a comparison of data during the calibration period, and the "δ-change" methods that take expected changes from model data and apply these to observed data. The properties of the calibrated data are therefore different depending on the method used. (See Section 2.2).

It is necessary to test thoroughly which method is best, and the details of this are given in what follows. In general, the testing procedure is based on the 'true world' analogy: model data for present and future periods are collected and one of several models is, in turn, designated 'observations' and a test of performance of various methods that transform the remaining models, one at a time, into those 'observations' is performed. The success of the particular method is evaluated from a closeness measure between the calibrated data and the known 'future observations' in the designated model.

Giving realistic scenarios of future frequencies of occurrence of cloudbursts requires special methods to be applied. This is because models do not represent cloudbursts as such, due to the sub-scale parametrization required: There are precipitation events in model data, of course, but actual realistic cloudbursts are absent (a cloudburst is defined in Denmark as

'at least 15mm of precipitation in half an hour'); this is due to the limited resolution of regional climate models, where convective events are parameterized as opposed to being modelled explicitly. The method chosen is simple but effective - it is based on a scaling between observed cloudburst frequency and hourly model-precipitation frequencies. This choice is based on the assumption that the modelled 1-hour mean-precipitation vs extreme-precipitation relationship does not alter form across time-scales.

Model data are available on a grid – in our case the CORDEX EUR model grid with a spacing between points of $0.11 \times 0.11°$ in a rotated coordinate system (roughly a 12.5×12.5 km grid, in Denmark). Observations are typically available as station series, or as interpolated products. The grid of the observations are typically not the same as used in the models and special considerations have to be made.

First of all, it is important to realise that some climate indices (typically those dealing with extremes) should not be derived from already interpolated data, due to a specific smoothing problem – interpolation does not preserve extremes. Rather, climate indices should be derived at the station level and then an interpolation of that index into a grid-product could be performed. This is not always possible. For instance, particular extreme indices may not have been considered at the time of generating the grid of observational data, and the original observed data may not be easily accessible for re-evaluation.

In addition, *Klimaatlas* delivers information at a resolution level that is useful to the endusers. The grid known as 'det Danske Kvadratnet' [Danmarks Statistik, 2019], which has a 1x1 km resolution, and is used in the "Klimagrid Danmark" dataset to be described in section 2.1 below, is used to provide information at high granularity, by interpolation in the CORDEX grid.

Klimaatlas therefore strives to deliver calibrated data, and then to output several dataformats that address the above expectations.

2.1   Dataset 'Klimagrid Danmark'

The Danish Meteorological Institute operates measurement stations for temperature and precipitation, and other observables, across Denmark. The observational data were used to produce evenly-spaced grids of data (10x10 km for precipitation, and 20x20 km for temperature) called 'Klimagrid Danmark' data ('KGDK' from now on) [Scharling, 1999, 2012, Wang and Scharling, 2012]. The grid used in KGDK is locked to the 'det Danske kvadratnet' grid [Danmarks Statistik, 2019].

Figure 1 shows the locations of the grid-points that make up the precipitation grid (10x10 km) in KGDK.

It should be noted that, in order to match DMI official climate normals for mean precipitation, we are using KGDK precipitation data that are not corrected for undercatch.
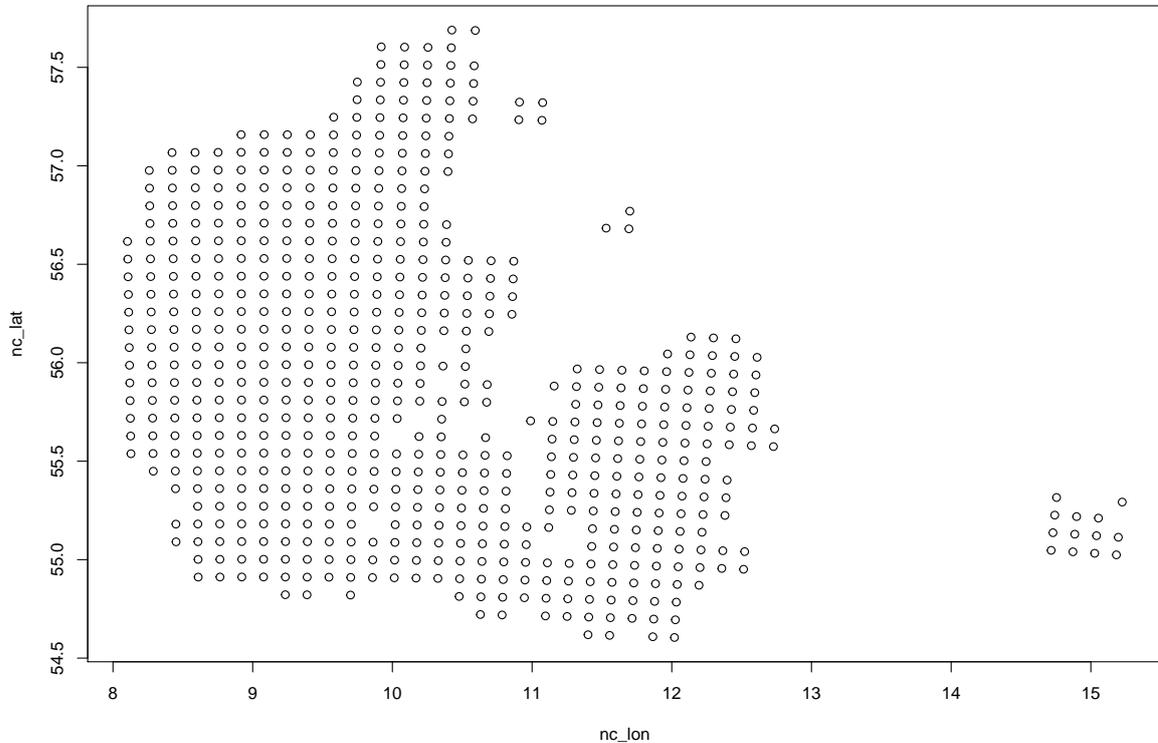
Figure 1: The Klimagrid Danmark grid for precipitation. Note that both Anholt and Læsø are represented.

2.2 Nomenclature

Figure 2 explains some of the nomenclature used in this report. A model variable is denoted M. The different periods are indicated with sub-scripts: M_c, M_r, and M_f refer to model values in the calibration period, the reference period, and the future period, respectively. In the calibration period we have simultaneous values of the model M_c and observations O. The calibrated model values in the reference period and the future period are denoted $\tilde{M}_r$, and $\tilde{M}_f$.

There are two over-arching types of calibration methods. The first type is denoted δ-change and is based on a mapping $M_c \to M_f$. This mapping is then applied to O to get $\tilde{M}_f$: $O \to \tilde{M}_f$. The other method is known as bias correction. This is based on a mapping $M_c \to O$ which is then applied to M_f to get $\tilde{M}_f$: $M_f \to \tilde{M}_f$.

In Sections 3 and 4 we will describe a set of calibration methods and test them via cross-validation based on CORDEX models. Based on these tests we will determine the calibration methods to be used in *Klimaatlas*. Note that we here are interested in calibration of time-series, and therefore use empirical methods. The study of extremes in precipitation (see section 4) and sea-levels (section 5) uses analytically based methods since a theoretical basis exists for the distribution of extremes.

Figure 2: Different time periods used in this work, and nomenclature.

3   Calibration of time series

3.1   The calibration methods

For both the δ-change and the bias-correction methods a mapping is determined from the calibration period. The mappings will be based on the distributional properties of the time-series, but will be applied to the time-series themselves. However, the mappings we will use are all monotonic. The δ-change method will therefore result in a bias corrected series, $\tilde{M}_f$, that preserves much of the temporal structure of the observations. On the other hand, the bias correction method will result in a series that preserves the main temporal characteristics of the model. This may be important to some users as the temporal characteristics of the model are not always realistic. A draw-back of the δ-change method is that the length of $\tilde{M}_f$ is limited by the length of the calibration period.
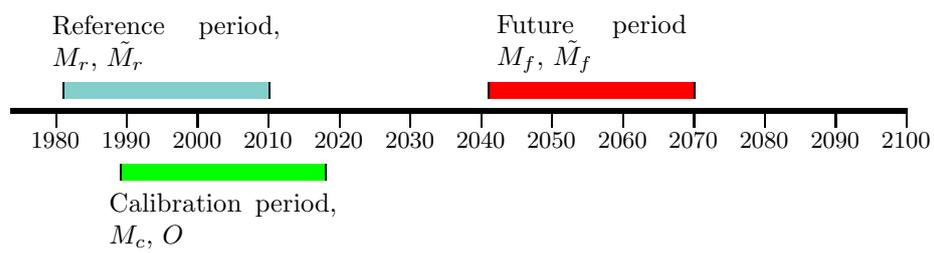
For both the δ-change and the bias correction methods a number of mappings can be chosen. The simplest is the additive mean correction. Here the bias correction mapping is given by $\tilde{M}_f = M_c + \overline{O} - \overline{M}_c$. This makes good sense for temperature while for precipitation the multiplicative mean correction $\tilde{M} = M_c\overline{O}/\overline{M}_c$ makes more sense. Overline denotes temporal means.

The mean corrections do not take care of the higher order moments such as the variance. To this end we consider quantile-quantile mappings ('q-q' from now on). Let F_O and F_{M_c} be the cumulative distribution functions of observations and the corresponding model variable in the calibration period, respectively. Then $\Xi = F_O^{-1}(F_{M_c})$ is the mapping for the bias correction method and the calibrated values are $\tilde{M}_f = \Xi(M_f)$. Note that the distribution of $\Xi(M_c)$ is per definition identical to the distribution of O. For the δ-change the mapping is $\Xi = F_{M_f}^{-1}(F_{M_c})$ and the calibrated values $\tilde{M}_f = \Xi(O)$.

In particular for the q-q mappings there are in practice a number of choices that have to be made. These include the number of quantiles used to represent the cumulative distribution functions (if the lengths of the series are identical then number of quantiles can be the length of the series). Another important choice is the type of extrapolation used for values that fall outside the values of the calibration period (Figure 3). We force the extrapolation to pass through origin for variables wind (max and mean), shortwave radiation and evaporation. In Figure 4 we show the resulting inclinations for precipitation and temperature for RCP8.5. Evidently, RCP8.5 models are on average wetter (notably winters) and cooler (notably summers) than observations. No inclinations are extremely large, and we expect the method to be robust.

We must also decide if we want to work on daily or monthly values even if only monthly results are needed.

For the precipitation a particular problem arises regarding the treatment of wet days and dry days. After some testing we have chosen the following simple and robust method. We adjust model precipitation series to replicate the fraction of wet days in the calibration period.
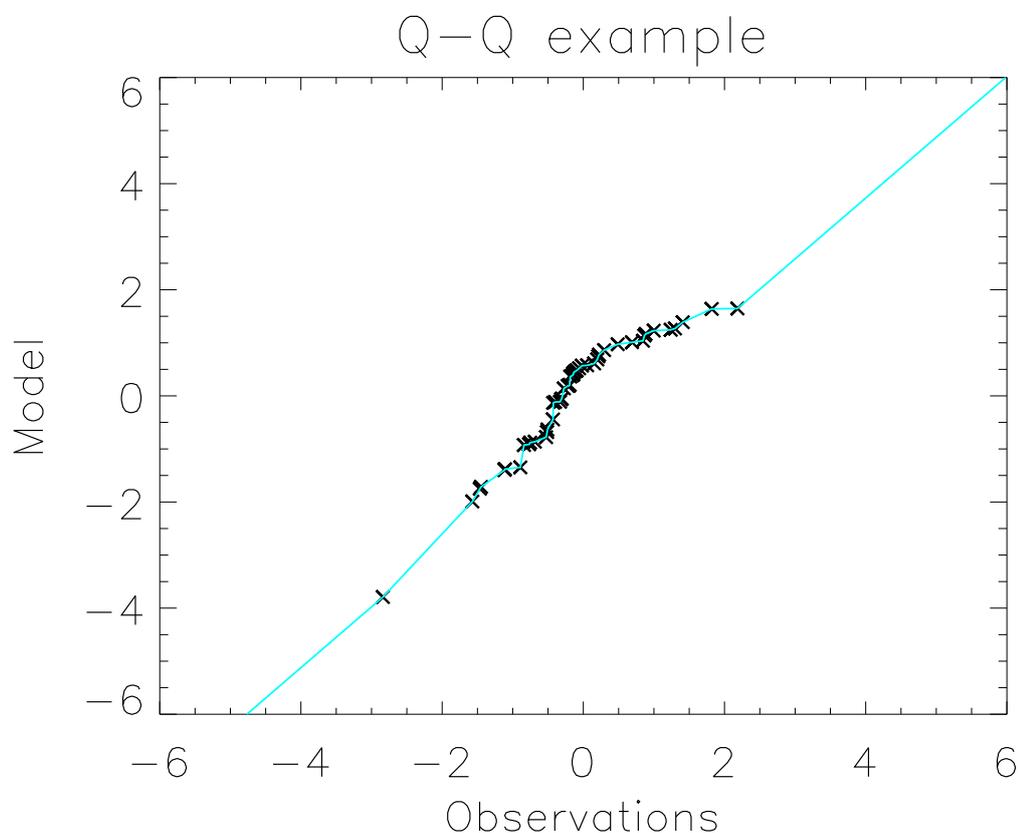
Figure 3: An example of how to extend the *q-q* map into the region without data. In this figure the last points to each side are extended with a straight line with the slope of the least squares line fitted robustly through all the points, which was our adopted method to deal with the ends of the distributions. Since version 2021a we have changed to a modified method whereby the low extremes, for some variables (see section 3.1 for details) are extrapolated with a line through (0,0) which helps avoid negative values where none ought to be possible.

In the case where the model has more wet days than observation, the days with the lowest model precipitation will be converted to dry days. In the opposite case, we promote modelled dry days to wet days by promoting days with the highest sub-threshold precipitation to the threshold precipitation amount; if necessary, random dry days will be similarly promoted.

3.2   Cross-validation

We determine the best methods by cross-validation based on 15 CORDEX models. The models are shown in Table 3 and we have data from historical experiments and the scenarios RCP4.5 and RCP8.5.
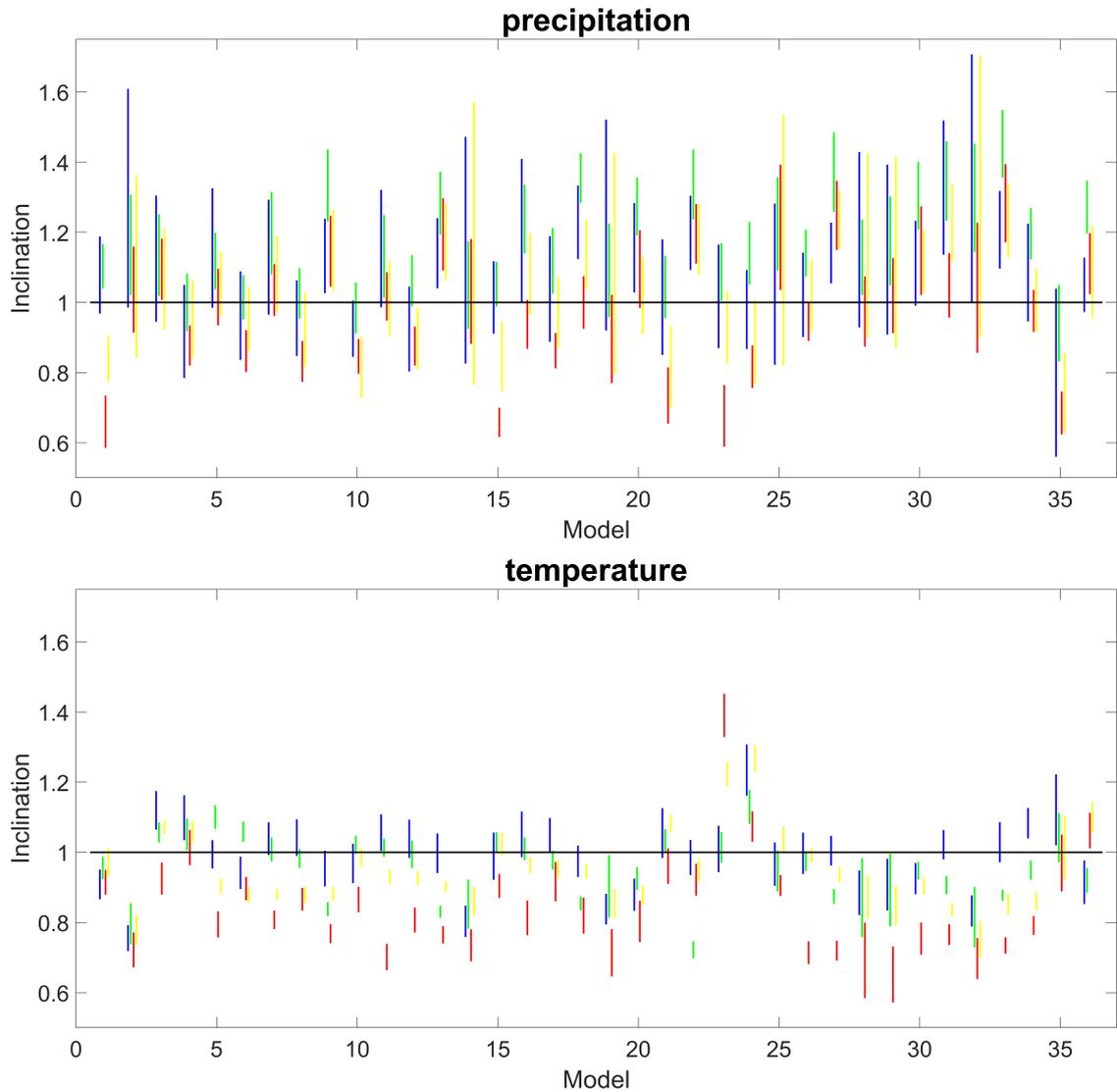
Figure 4: For RCP8.5 we show the inclinations of the robustly fitted lines used in the q-q mapping extensions, as explained in Figure 3. Top panel shows for precipitation while bottom panel shows for temperature. The coloured lines indicate seasons. Green is spring, red is summer, yellow is autumn, and blue is winter values. The length of the lines indicate spread over models.

Table 3: List of the 15 CORDEX model combinations used in the cross-validation experiments aiming on determining best method for time-series calibration. As *Klimaatlas* is continuously updated, these models are a subset of what is currently used in the atlas – see Table 7 for the current list.

	Global model	Regional model
0	MPI-M-MPI-ESM-LR	CLMcom-CCLM4-8-17_v1
1	MPI-M-MPI-ESM-LR	MPI-CSC-REMO2009_v1
2	MPI-M-MPI-ESM-LR	SMHI-RCA4_v1a
3	CNRM-CERFACS-CNRM-CM5	CLMcom-CCLM4-8-17_v1
4	CNRM-CERFACS-CNRM-CM5	SMHI-RCA4_v1
5	ICHEC-EC-EARTH	CLMcom-CCLM4-8-17_v1
6	ICHEC-EC-EARTH	SMHI-RCA4_v1
7	ICHEC-EC-EARTH	KNMI-RACMO22E_v1
8	ICHEC-EC-EARTH	DMI-HIRHAM5_v1
9	IPSL-IPSL-CM5A-MR	IPSL-INERIS-WRF331F_v1
10	IPSL-IPSL-CM5A-MR	SMHI-RCA4_v1
11	MOHC-HadGEM2-ES	CLMcom-CCLM4-8-17_v1
12	MOHC-HadGEM2-ES	DMI-HIRHAM5_v1
13	MOHC-HadGEM2-ES	KNMI-RACMO22E_v2
14	MOHC-HadGEM2-ES	SMHI-RCA4_v1

In cross-validation a model is chosen to represent the 'truth' (observations). The remaining 14 models are then calibrated against this 'truth'. As data now exist for the 'truth' in the future the calibration method can be validated. The 'truth' can be chosen as each of the 15 models and this gives us 15*14 different combinations of 'truth'/model.

When comparing the calibrated models with the 'truth' we are interested in the distributional differences. These are here estimated with the mean, the standard deviation, and the Kolmogorov-Smirnov statistics. The latter measures the maximal distance between the two cumulative distributions and therefore provides an overall measure of the difference between the distributions.

We are interested in comparing simple mean adjustment and *q-q* transforms for both δ-change and bias correction.

3.3 Results

Figure 5 shows an example which demonstrates the difference between the δ-change and the bias correction. The top panel shows the time-series in the calibration period. Comparing the green and the blue curves we see that the model is too warm. From the bottom panel we see that this also holds in the future. In the bottom panel, the red curve is the bias corrected series, and the cyan is the δ-change calibrated series. We see that both the calibrated series fit the
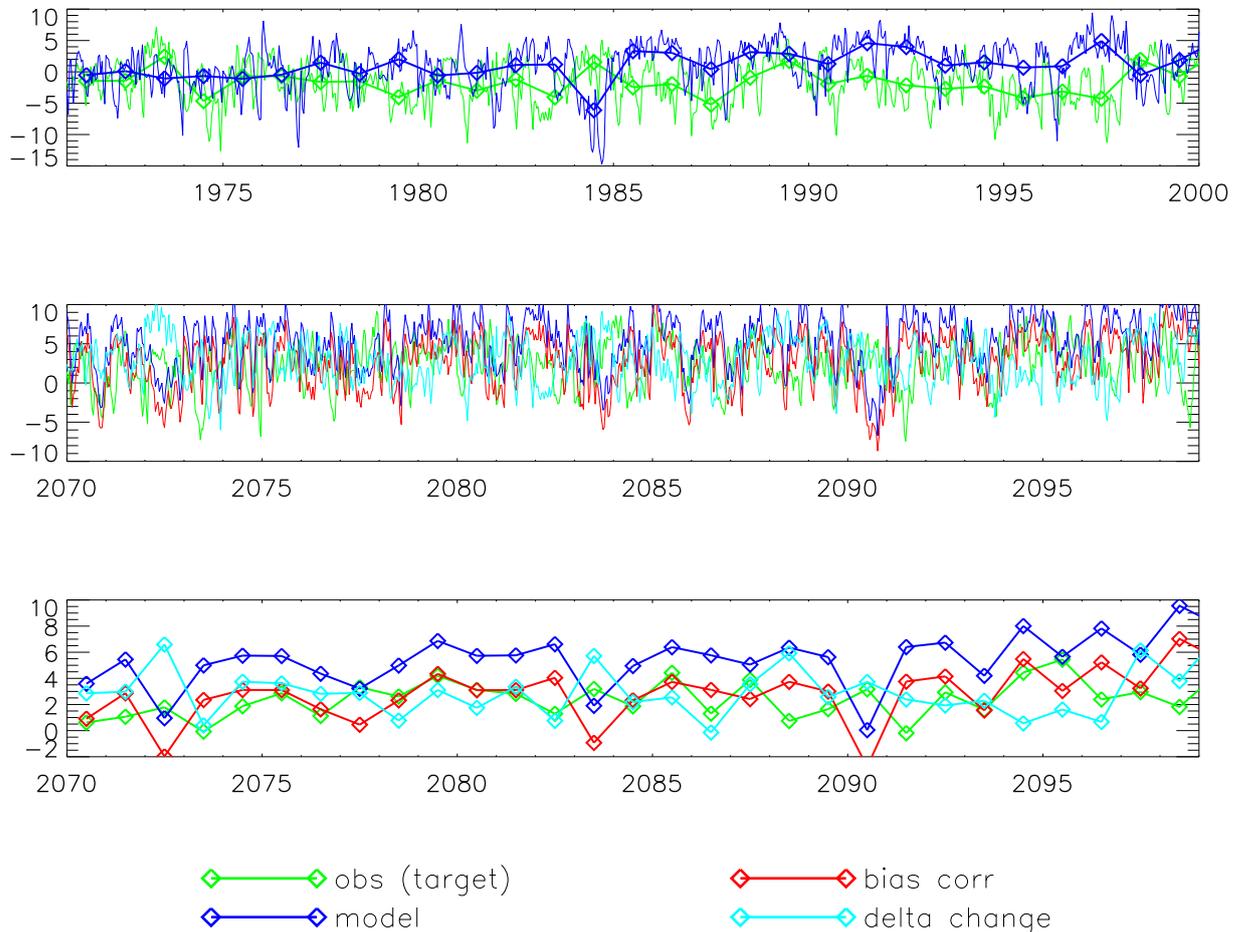
Figure 5: Time-series demonstrating simple mean bias correction. This is January near-surface temperature. Calibration period 1971-2000 (upper panel), prediction period: 2070-2099 (bottom panel). Scenario: RCP8.5. As observation is used model number 3, and for model number 14. Thick curves are monthly means, thin curves are daily values.

mean value of the 'truth' better than the uncorrected series. Note that we cannot be sure that this is always the case: the climate change in model and 'truth' could be different and conspire in a way to make the effect of the calibrations negative. Note, also as mentioned before that the δ-change calibrated series has the same temporal characteristics as the observations while the bias corrected series has the characteristics of the model.

We are now ready to describe the results of the cross-validation experiments. The next figures show results in a matrix form where the ordinate indicates the model chosen as 'truth' and the coordinate the model chosen as model. Figure 6 shows the difference of the mean climatology in the future between the calibrated models and the 'truth'. The top panel shows the difference without any calibration, i.e., just the difference between the model and the 'truth'. The second and third rows show the differences based on the calibrated values. In the second

Figure 6: The difference between mean climates in calibrated models and 'truth'. January near-surface temperature. Calibration period 1971-2000, prediction period: 2070-2099. Scenario: RCP8.5. The numbers on the axes refer to the model combinations in Table 2. The horizontal axes indicates the model selected as 'truth'. Top panel shows uncalibrated values. In middle panes calibration is performed on monthly means, in lower panels on daily means.

row the calibrations are done on monthly means, in the third row on daily values. Values close to zero are good. First, we note that any calibration is better than no calibration. Although not extremely obvious from these plots we find that in general bias correction is better than δ-change and that it is better to do the calibration on daily values than on monthly means. However, note that these conclusions hold for the average over many 'truth'/model combinations. There is a large scatter in the plots and for some combinations of 'truth'/model the calibrations have not improved the model.

Figures 7 and 8 show results for the difference between standard deviations and for the KS statistics. The KS-statistics is always positive and values close to zero indicate that the distribution of the two time-series are similar. The conclusions from the last paragraph based on the mean climates are confirmed.

Until now we have focused only on monthly means of the surface temperature in January in the late century. We summarise these results in plots like those in Figure 9. We also have results for precipitation, for other months, for other periods, and for daily means (not shown).

It is interesting to study the effect of the length of the calibration period. Figure 10 shows results for the settings as Figure 9 but for a shorter calibration period. We see that results have worsened and there is now only little difference compared to the situation without any calibration.

3.4   Conclusions

Based on the cross-validation experiments described above we draw the following conclusions:

- In general, bias correction seems to be the best method.

- Bias correction should be performed on daily data even if only monthly means are wanted.

There are some other considerations:

- Results are sensitive to length of calibration period, but in *Klimaatlas* the impact is minor since 30-year periods of calibration data are available.

- Bias correction gives temporal correlations as in model, not as in observations.

- For δ-change, the length of the calibrated series is limited by the length of the observations.

We emphasize that these conclusions hold only for the average over many realizations and the situation may be different for a particular 'truth'/model combination. The conclusions are probably somewhat on the optimistic side as they are based on model/model comparison and not on real observations.
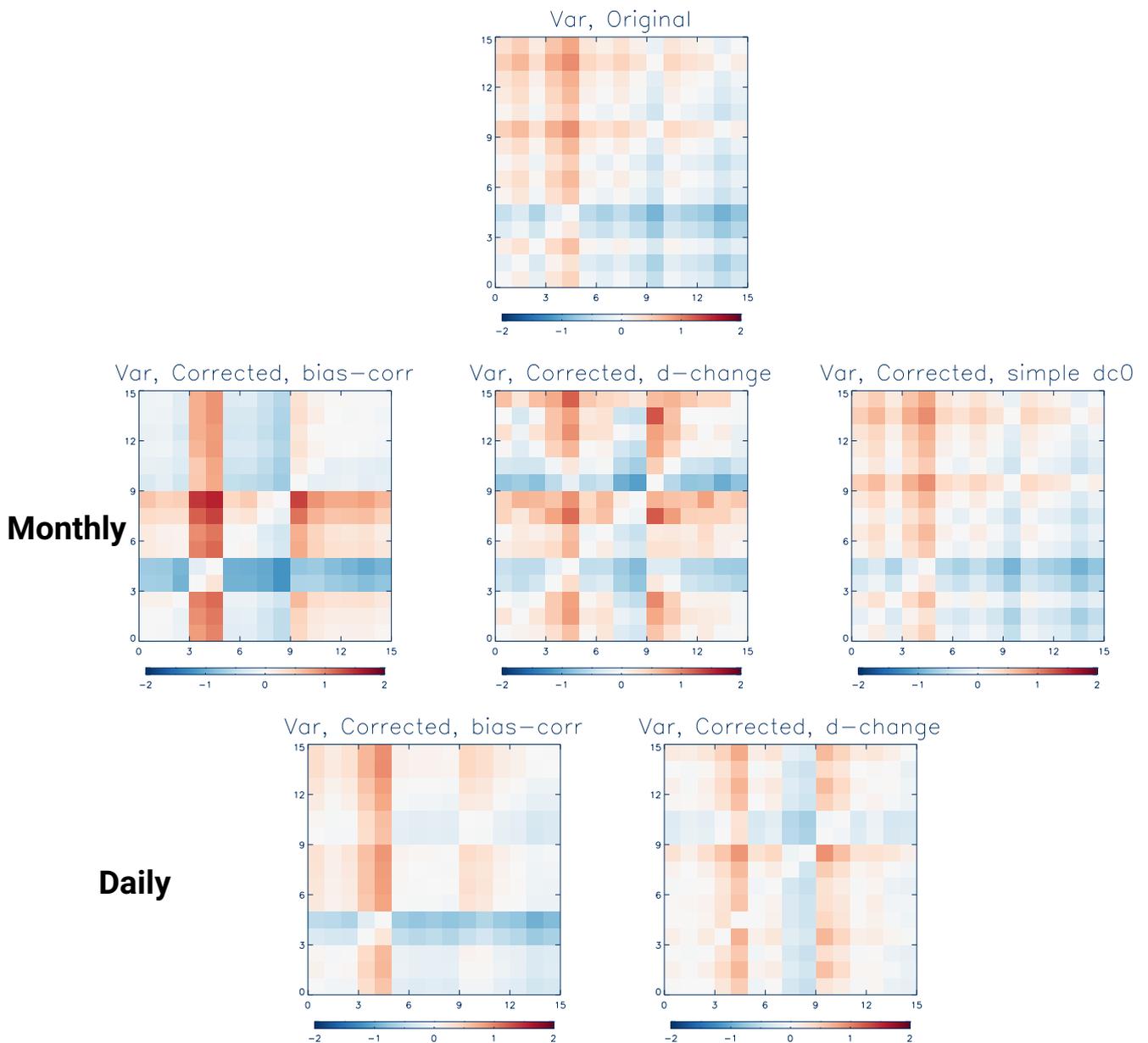
Figure 7: The difference between the variability (standard deviations) in calibrated models and 'truth'. January near-surface temperature. Calibration period: 1971-2000, prediction period: 2070-2099. Scenario: RCP8.5. The numbers on the axes refer to the model combinations in Table 2. The horizontal axes indicates the model selected as 'truth'. Top panel shows uncalibrated values. In middle panels calibration is performed on monthly means, in lower panels on daily means.
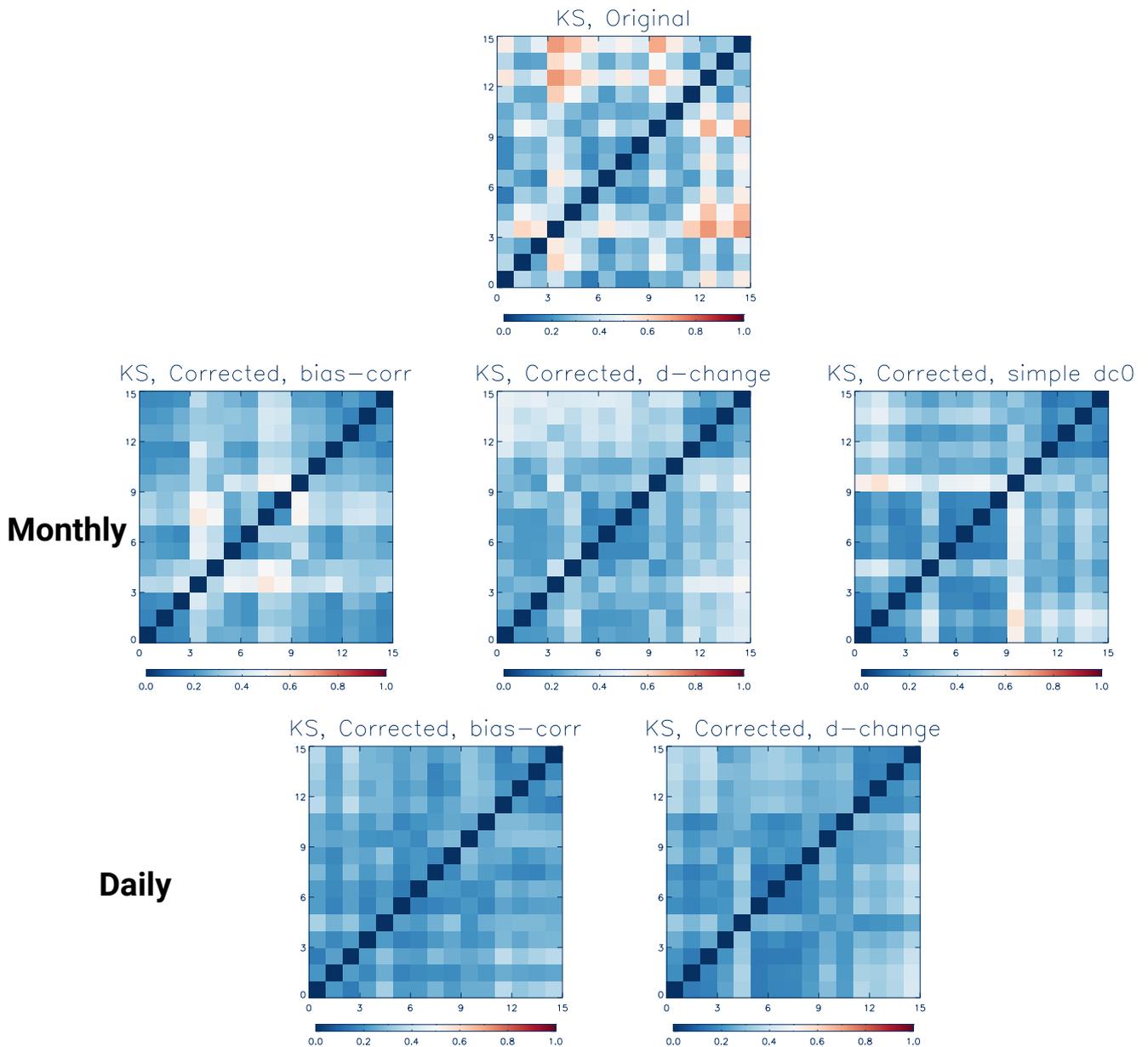
Figure 8: Kolmogorov-Smirnov statistics for January near-surface temperature. Calibration period 1971-2000, prediction period: 2070-2099. Scenario: RCP8.5. The numbers on the axes refer to the model combinations in Table 2. The horizontal axes indicates the model selected as 'truth'. Top panel shows uncalibrated values. In middle panes calibration is performed on monthly means, in lower panels on daily means.
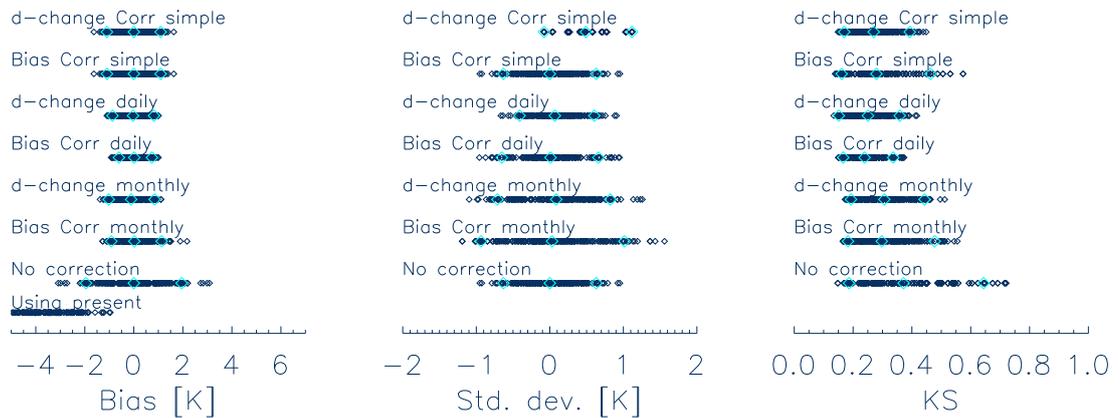
Figure 9: Summary of the cross-validation results for January near-surface temperature. Calibration period 1971-2000, prediction period: 2070-2099. Scenario: RCP8.5. The columns are: mean, standard deviation, and KS. For each method the 15*14 cross-validation results are shown by dots. Blue diamonds mark average, and upper and lower 5 percentiles.
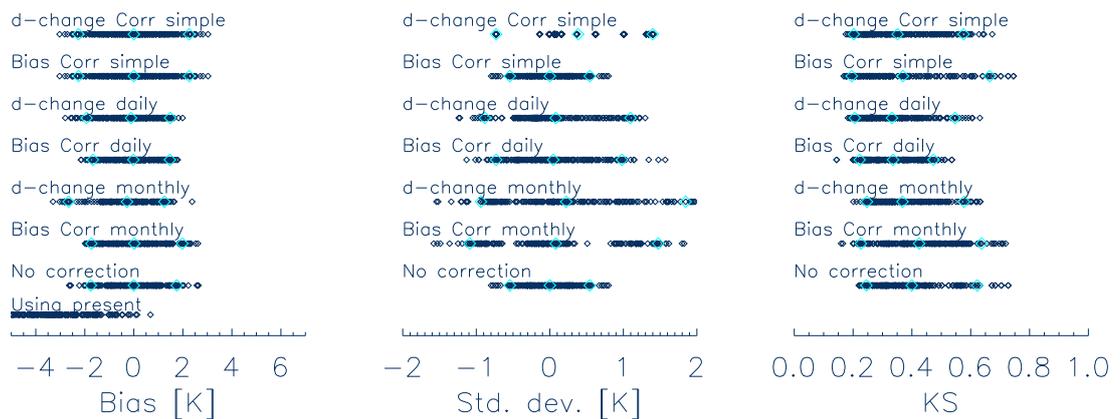
Figure 10: As Figure 9 but for a shorter calibration period, 1985-2000.

4   Calibration of extreme precipitation

4.1   Short introduction

Extreme events occur rarely and therefore the empirical quantile-quantile calibration technique
described in Section 3 cannot be used, since the tail of the empirical cumulative distribution
function (CDF) is poorly defined. Therefore, for extreme events, extreme value analysis is ap-
plied, where the empirical CDF is replaced by an analytically formulated cumulative distribution
function, as described below.

   This work has been published [Schmith et al., 2023].

4.2   Extreme value analysis

 In extreme value analysis (EVA) one considers a time series of e.g. hourly values, and the aim
is to estimate the frequency of occurrence of rare events, often expressed as the T-year return
level, which is the level that on average is exceeded once every T years.

   We use the peak-over-threshold (POT) method, where all peak values above a specified
threshold x_0 and separated by a minimum time span are considered. It is assumed that peak
occurrences are independent and Poisson-distributed with parameter λ, which is the average
number of exceedances (events) per year. Alternatively, λ can be specified, in which case x_0 is
a stochastic variable.

   It can be shown that under very general conditions the distribution of the peak exceedances
$x - x_0 > 0$ are distributed as a Generalised Pareto distribution (GPD) with cumulative distribu-
tion function given by

$$F_{GPD}(x - x_0) = 1 - \left(1 - \xi \frac{x - x_0}{\sigma}\right)^{1/\xi}, x > x_0. \tag{1}$$

   The T-year return level is determined as the level exceeded on average once every T years,
and therefore the following holds:

$$\lambda T[1 - F_{GPD}(x_T - x_0)] = 1 \tag{2}$$

from which we get

$$x_T = F_{GPD}^{-1}(1 - \frac{1}{\lambda T}) + x_0. \tag{3}$$

   There are several procedures available for estimating the parameters from data, the most
important being: maximum likelihood (ML), method of moments (MOM) and probability-
weighted moments (PWM). Hosking and Wallis [1987] and Hosking et al. [1985] demonstrate

that PWM in general yields reliable results with low variance for the number of samples in this study, whereas in particular ML can be problematic. Therefore we use PWM in the following. For more details see Coles [2001].

4.3   Analytical quantile matching

In Section 4.2 the theoretical framework was presented for estimating extreme value distributions and associated return levels. This can be applied to obtain future projected values and climate factors, defined as the ratio between a future and a present value, which will be presented below.

We make use of Equation 3 above, which is valid both for M_c and for O and for any return period T. If we apply this to O and M_c we obtain the expression

$$(1 =)\lambda_{M_c}T[1 - F_{GPD,M_c}(M_{c,T} - M_{c_0})] = \lambda_O T[1 - F_{GPD,O}(O_T - O_0)] \tag{4}$$

relating $M_{c,T}$ and O_T, and after some manipulation, we arrive at

$$O_T = F_{GPD,O}^{-1}\left\{1 - \frac{\lambda_{M_c}}{\lambda_O}\left[1 - F_{GPD,M_c}(M_{c,T} - M_{c_0})\right]\right\} + O_0 \tag{5}$$

Thus, Equation 5 defines a transformation from $M_{c,T}$ to O_T, which then in the calibration procedure is applied to $M_{f,T}$ to obtain $\tilde{M}_{f,T}$.

4.4   Practical implementation

4.4.1   POT-parameters from observations

We follow closely the method described in [Gregersen et al., 2014b,a, Madsen et al., 2017]. In this method, the local, geographically varying parameters in the POT are given for 1 and 24 hours duration as linear functions of explanatory variables, derived from gridded daily precipitation totals from Klimagrid Danmark over the period 1989-2010 see (section 2.1) using regression. The explanatory variables are: 1) the mean annual precipitation and 2) the mean daily exceedances over a threshold of z_0 = 19.2 mm/day. Using mean exceedances is an alternative formulation of the GPD distribution. The regression coefficients linking the Poisson parameter, and mean exceedances (equivalent to the scale) are given in Gregersen et al. [2014b], while the shape parameter has been given by Gregersen (pers. comm.)

4.4.2   POT parameters from models

EVA was done on precipitation data from a number of different GCM-RCM combinations – see Table 8. These have in general different precipitation characteristics. Therefore, we use a different censoring than for the observations, in that we specify λ = 3 events/year and determine

a z_0, varying spatially and between models. Peaks in the rain intensity should be separated by 24 hours or more to count as separate events. We estimate the parameters in every grid point in KGDK. Subsequently, the shape parameter is area-averaged before being used.

4.5   The final procedure

According to Equation 5 a transformation is established from the present-day model to the observations based on the analytical quantile mapping. Subsequently this transformation is applied to return levels from the scenario to give as output calibrated future return levels.

The Climate Atlas provides return levels for 2, 10 and 100 year return levels, and for 1 h- and 24 h-summed precipitation values[1].

4.6   Cloudbursts

The definition of a cloudburst is, as stated before, precipitation exceeding 15 mm in 30 minutes, but none of the CORDEX models have this temporal resolution represented in their output. Therefore an alternative approach has been chosen. In the DMI Technical Report 19-06 [Cappelen, 2019], station observations in high temporal resolution have been analysed for the period 2011-2018. In an average year, 87 stations out of 258 have measured at least one cloudburst. This roughly corresponds to one every 3 years for the given network of stations, ignoring any regional variation in the probability. The 'calibration period' for cloudbursts is therefore 2011-2018.

With the assumption that the occurrence of cloudbursts is associated with extremes in hourly precipitation, which is readily available from models, we use hourly precipitation with a present-day return period of 3 years as a proxy for the occurrence of cloudbursts.

The change in 3-year return-level in hourly precipitation can be obtained from the parameters of POT fits to present-day and future extreme precipitation. From the present-day parameters, the three-year return level can be obtained for each point. This value is now entered into the corresponding CDF for the future period, and the return frequency of this value can be calculated. The uncertainty is calculated as the pointwise spread among models.

4.7   Software Flowchart

The atmospheric-data methods described above are shown in diagrammatic form in the flowchart in Figure 11. The data resulting from these procedures are stored.

---

[1]Since this initial analysis, Climate Atlas has been expanded and now provides 2, 5, 10, 20, 50 and 100 year return levels for 1 and 24-hour precipitation.
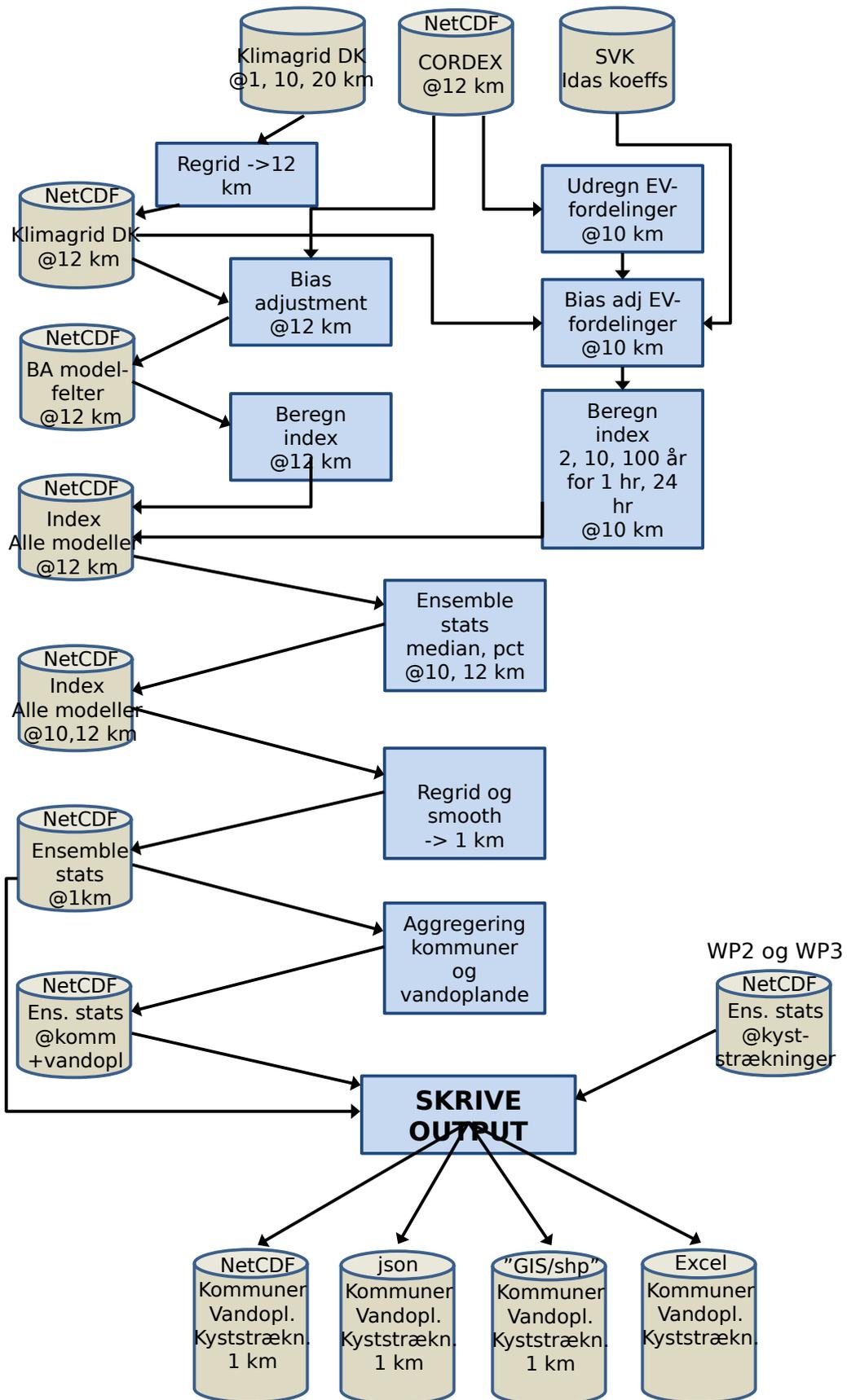
Figure 11: Flowchart showing the atmospheric-data processing steps.

5 Mean sea level rise

5.1 Introduction

Information on climate change is assessed by IPCC. In 2013, IPCC released its 5th assessment report (AR5), giving the best estimates and likely ranges of sea level change on global and regional scale [Church et al., 2013b]. In 2019, IPCC released a Special Report on the Ocean and Cryosphere in a Changing Climate (SROCC) [Oppenheimer et al., 2019]. In SROCC, two important aspects of sea level are noted initially for understanding the climate change-induced sea level rise (SLR): climate change-induced global mean sea level (GMSL) rise (introduced in this section) and extreme sea level (ESL) rise (Section 6). In August 2021, IPCC's most current report, the sixth assessment report (AR6) from Working Group I (WGI), was released [Fox-Kemper et al., 2021]. In AR6 WGI, IPCC offers policymakers regular scientific assessments of climate change, its consequences, and future risks. As part of this initiative, IPCC reviews and synthesizes scientific literature and publishes consensus projections of future sea levels around the globe for a variety of possible future scenarios.

5.1.1 "Representative Concentration Pathways"(RCPs) and "Shared Socioeconomic Pathways"(SSPs)

Different modelling groups in IPCC are tasked with exploring how the globe could evolve during the rest of the 21st century. The "Representative Concentration Pathways" (RCPs) were devised by a group of scientists to describe the different amounts of greenhouse gases and other radiative forcings that may occur in the future. RCP2.6, RCP4.5, RCP6.0, and RCP8.5 are four scenarios that encompass a wide range of forcing in 2100 (2.6, 4.5, 6.0, and 8.5 watts per meter squared). A second group modelled how socioeconomic factors may evolve over the course of the next century. These factors include population, economic expansion, education, urbanization, and the rate of technological advancement. Five narratives describing different development paths of society were designed. These five "Shared Socioeconomic Pathways" (SSPs) examine how the world may evolve in the absence of climate policy and how varying degrees of climate change mitigation could be accomplished when the RCPs' mitigation aims are linked with SSPs.

The two modelling groups were designed to complement one another. The RCPs provide pathways for greenhouse gas concentrations and the amount of warming that might take place by the end of the century. Whereas the SSPs set the framework for whether or not the emission reductions will be achieved. The SSPs, which were first released in 2016, are just now beginning to be included into the latest cycle of climate modelling, known as the Coupled Model Intercomparison Project version 6 (CMIP6), for the IPCC AR6. Five scenarios will be used for standard runs in CMIP6 for a worldwide agreement, with the designation of individual scenar-

ios consisting of the name of the fundamental pathway followed by two numbers indicating the extra radiative forcing attained by 2100. SSP1-1.9, SSP1-2.6, SSP2-4.5, SSP3-7.0, and SSP5-8.5 are their designations. SSP1-2.6/RCP2.6, SSP2-4.5/RCP4.5, and SSP5-8.5/RCP8.5 are the three scenarios included in Climate Atlas' mean sea level projections in version 2022. To be consistent with earlier versions of Climate Atlas, we continue to utilize RCPs in the following text. Note that in version 2022 we also included the "deep uncertainty" part of all the scenarios.

From IPCC SROCC through IPCC AR6, the uncertainty in sea-level estimates has been communicated differently. The AR6 projections with *medium confidence* contain estimated distributions for each emissions scenario and two distinct methodology options for the Antarctic ice sheet. AR6 also included a set of projections with *low confidence*, which included additional contributions from ice sheet processes and estimates with less agreement and/or less evidence. From the perspective of risk perception, it is essential to comprehend how the highest assessed SLR for each area compares with an estimate from the upper tail of the probability distribution of IPCC regional SLR projections, given that such scenarios, if realized, would be very devastating. Successful adaptation methods need significant preparation in advance to be effective in this worst-case scenario. Thus, the Climate Atlas 2022 version uses scenarios with *low confidence* to present the upper-level SLR estimate as the worst-case scenario. The details of this "deep uncertainty" part are described in Section 5.2.3.

5.1.2 Global mean sea level rise

There are clear links between rising temperature and GMSL rise. Observed and projected GMSL rise has two major components; thermal expansion (increase in the volume of ocean water caused by additional heat uptake) and meltwater input to the ocean from retreating land-ice (glaciers and ice sheets). Other contributions include for example changes in land water storage. The thermal expansion effect is included in coupled ocean-atmosphere climate models. The meltwater input from ice sheets is presently not included in the global climate models assessed in SROCC and AR5, but is added to the GMSL signal afterward [Slangen et al., 2017]. In SROCC, it is clear that Antarctica is a source of major uncertainty in the estimation of future SLR, and will have a positive net contribution to GMSL rise.

To get a better understanding of the meltwater input from ice sheets, intense research is ongoing internationally, and it is expected that more precise knowledge will become available in the coming years. At present, it is internationally acknowledged that there is a small but not negligible risk of large and rapid changes especially from Antarctica, which would lead to rapid sea level rise (e.g. [DeConto and Pollard, 2016, Bamber et al., 2019]), and that sea level rise will continue for centuries, with a speed that heavily depends on greenhouse gas emissions [Oppenheimer et al., 2019].

5.1.3   Local sea level rise around Denmark

Sea level change is not evenly distributed around the globe. Differences occur mainly due to gravitational and elastic effects in relation to melting ice (regional scales), effects of regional ocean dynamics (changes in current systems) and regional steric effects (that is, ocean volume changes due to regional changes in temperature and salinity).

Changes in the Earth's gravity field and elastic deformation of the solid Earth give rise to spatial differences in the sea level rise pattern [Mitrovica and Milne, 2003]. For example, near an ice sheet losing mass in the Antarctic, reduced gravitational attraction between the ice and the nearby ocean causes the sea level to fall, despite the global sea level rise [Mitrovica et al., 2011]. In the Climate Atlas, we adopted the factor of 1.1 for the sea level signal from Antarctica for the whole of Denmark, following the sea level fingerprint from Mitrovica et al. [2009], which is the same as in the AR6 SLR datasets.

Regional ocean dynamics, that is, ocean currents, have an associated sea level signal. For instance, the Gulf Stream has a sea level signal of about 1 m. A change in ocean currents will have an impact on sea level change. Similarly, a change in the average wind patterns in coastal areas changes the push of the wind on the water towards the coast, giving rise to local sea level change. The dynamic effects are included in ocean models of climate change depending on the scales resolved.

Regional steric effects occur if the salinity of the regional ocean changes, or the change in temperature is different from the global mean. The effects are included in ocean climate models.

The local coastal sea level ($\sim$ 10km) is affected by global, regional ($\sim$ 100km) and coastal features (e.g. regional land rise and local subsidence).

Regional/local land rise in Denmark has been assessed by DTU Space. Overall, all of Denmark is rising due to glacial isostatic land rise in Scandinavia after the last ice age. The land rise of northern Denmark is about 2 mm per year, decreasing towards south and west, to zero just south of the Danish border (Personal communication, Per Knudsen, DTU Space, 2016). In the past, this has compensated for external sea level rise, giving an average relative sea level decrease in the northern-most part of the country in the 20th century [Hansen, 2018].

5.1.4   Observed mean sea level and change

Globally, GMSL of the last centuries is well documented, including acceleration after the 19th century [Church et al., 2013a, Bamber et al., 2018]. Over the last two centuries, estimated GMSL rise mostly relies on coastal tide-gauge measurements. The average estimate is 1.4 mm yr^{-1} for the period 1901-1990 based on two recent reconstructions by Hay et al. [2015] and Dangendorf et al. [2017]. High precision satellite altimetry started in October 1992, providing altimetry-based ocean wide estimates of GMSL rise. Average GMSL increased to 3.2 mm yr^{-1} over the period 1993-2015 [Watson et al., 2015, Nerem et al., 2018]. In AR6, IPCC provides the GMSL during the most recent period analyzed, 2006-2018, it's been rising at a rate of 3.7

mm yr^{-1}, nearly three times as fast as during 1901-1971 (1.3 mm yr^{-1}). Therefore, IPCC AR6 concluded that, "since 1900 the sea level rise has greatly accelerated (*high confidence*)".

In Denmark, the local sea level has been measured with tide gauges since the end of the 19th century. Monthly and annual mean sea level from the 14 stations with more than 20 years of data is published in Hansen [2018] and reported to PSMSL [Holgate et al., 2013]. Sea Level is measured relative to a local datum, which can be directly converted to the Danish national height system DVR90. This was designed to approximately match the mean sea level around Denmark in 1990. The mean sea level of the Climate Atlas reference period (1981-2010) for the 14 stations in Hansen [2018], relative to DVR90, is listed in Table 4. However, these numbers should be used with some care, as many data are missing, especially from the 1980'es. This introduces a high bias, as the sea level has generally been rising throughout the period.

Table 4: Relative mean sea level (cm) at 14 Danish stations 1981-2010, height system DVR90, derived from Hansen [2018]. Years with more than 10% missing data have been left out in the calculation.

Station	Sea level [cm]	Station	Sea level [cm]
Hirtshals	-7	Slipshavn	3
Frederikshavn	-5	Korsør	5
Hanstholm	-1	Hornbæk	4
Århus	2	København	8
Fredericia	1	Rødbyhavn	6
Esbjerg	7	Gedser	7
Fynshav	1	Tejn	2

5.2   Methods

5.2.1   Dedicated modelling effort

We performed the HBM climate simulations for five periods, i.e. historical period, 1981-2010; RCP 4.5 period, 2041-2070; RCP 4.5 period, 2071-2100; RCP 8.5 period, 2041-2070; RCP 8.5 period, 2071-2100. For a detailed description of HBM please refer to Section 8.2.2.

Ensemble simulations using EURO-CORDEX members are ongoing throughout the Climate Atlas project. Before the Climate Atlas release 2019, we were able to perform two simulations using the meteorological forcing from two CORDEX members: DMI-HIRHAM5_v1 (Nr. 8 and in Table 3) and SMHI-RCA4 (Nr. 6 and in Table 3). In version v2020b, we have added one additional experiment based on CORDEX member DMI-HIRHAM5_v2.

5.2.2   Localising global mean sea level rise

A general introduction to local sea level rise around Denmark is given in Section 5.1.3. Here we present how to obtain the local sea level rise values. The localizing methodology using AR6

data has less steps as in previous Climate Atlas releases, which follows the work using AR5 data described in Olesen et al. [2014], and the main procedure is as listed below.

1) Obtain the electronic data based on Fox-Kemper et al. [2021] through the NASA/IPCC Sea Level Projections Tool at `https://sealevel.nasa.gov/ipcc-ar6-sea-level-projection-tool`. The sea level projections in AR6 are produced by a package named the Frameworks for Assessing Changes To Sea-level [FACTS, Garner and Kopp, 2022]. The data includes the median value (50%), textitlikely range (upper 83% and lower 17% limits) and the *very likely* range (upper 95% and lower 5% limits).

2) In the first step of the data processing, glacial isostatic adjustment (GIA) is deducted, since more detailed regional land rise is used in Climate Atlas (Section 5.1.3).

3) Scale to the Climate Atlas reference period. In Climate Atlas, we used reference period 1981 - 2010 and 30 year time slices. However, all the IPCC SLR projections used the reference period 1995 - 2014 and 20 year time slices. Therefore, the projected SLR is scaled to the Climate Atlas reference period according to a quadratic formula.

4) The importance of mean sea level change caused by local ocean dynamics and steric effects has been evaluated by averaging 30 years of sea level data from HBM simulations for each period. We found this contribution at the end of the century varies between -1.5 cm and -0.4 cm . We, therefore, considered this change within the uncertainty range, and thus too small to be significant. It has been left out of the further calculations.

5) The IPCC AR6 report provides both the likely range (17% to 83%) and the very likely range (5% to 95%), whereas the previous IPCC report only provided the likely range. It can be advantageous since it provides a more complete view of the projected sea level rise. For Climate Atlas, we used a very likely range with lower and upper limits being 10 and 90 percentiles. We discovered that using 95% upper bound estimates from IPCC AR6 for Denmark needs further investigation. As a result, we keep to the methods employed in prior versions of Climate Atlas, which are as follows. It is considered a good approximation of the IPCC's very likely lower bound estimates (5%). Based on a symmetric normal distribution, we derived the 90 percentile from the likely range of IPCC AR6 (83%). The method should provide a lower estimate of the very likely uncertainty than the IPCC AR6 method, particularly for the RCP8.5 scenario, but it was chosen since it is simple and well-described.

6) All values were corrected for the regional land rise, to provide the relative sea level signal, according to section 5.2.5.

5.2.3   The low-confidence and high-impact scenario

There is a small but significant risk of rapid sea level rise outside the likely estimates, which is mirrored in relatively high numbers for the upper percentiles for a global-sea level because of the uncertainty of ice-sheet-processes. In an effort to also account for uncertainty in systems that we cannot confidently model, IPCC AR6 now divides uncertainty into two types, normal uncertainty and deep uncertainty. Likely range projections do not include those ice-sheet-related processes whose quantification is highly uncertain or that are characterized by deep uncer-

tainty. Note that this uncertainty is asymmetrical. For evaluating this uncertainty, they employ both a poll of experts and a smaller, more specific organized expert opinion. AR6 now incorporates this sort of expert opinion to evaluate risks that cannot be properly modelled but yet cannot be disregarded. In addressing the climate risks, it is not sufficient to examine what is likely to occur; it is much more crucial to comprehend what the risks are.

The present consensus on particularly the higher percentiles (95% and above) is that they cannot be constructed meaningfully by statistical analysis of data from the existing climate model ensembles, nor can they be constrained by dedicated model efforts. This is in part due to the lack of interactive glacier and ice sheet modules in the applied climate models and partly due to a limited physical understanding of the processes that have been suggested to lead to instabilities in the Antarctic Ice sheet as ocean and atmospheric temperatures increase. The latter includes two independent steps whereby the established impact of global warming is a loss of the floating ice shelves which in the following phase leave tall ice cliffs exposed that will collapse under their own weight; a process termed marine ice-cliff instability. This idea was first proposed by DeConto and Pollard [2016] and have been integrated into a very recent expert assessment addressing the high end percentiles [Bamber et al., 2019].

This expert judgment concludes that for a five-degree warming there is a 5% risk that global mean sea-level will exceed 2.4m year 2100, where 1.8m is directly linked to ice sheet melting. This study appears to be contradicted by the more recent high-impact paper by Edwards et al. [2019] that demonstrates that the proposed critical instability is far from certain and has likely not been in play during warm climates of the past. A full review on the topic is not the intention here, but in deciding on the recommendations here, consultations with Danish experts have been important. It is with this background the expert elicitation of Bamber et al. [2019] is chosen as the basis for a 95% percentile estimate. It is further the judgment that the experts contributing to the assessment were indeed informed about the forthcoming results by Edwards et al. [2019] and that this knowledge has been incorporated into their judgment. It should also be noticed that 10% and 90% percentiles from Bamber et al. [2019] are largely consistent with AR6's very likely ranges.

In order to try to account for uncertainty in processes that we are unable to predict with complete confidence, the IPCC AR6 has now separated the uncertainty into two distinct categories, named medium confidence and low confidence scenarios. Within our calculation in Version 2022, we already included the "deep uncertainty" range of IPCC AR6 low-confidence and high-impact scenarios. As global SLR is both one of the most certain (the sea level will rise) and uncertain (with regards to the range of the SLR) components of climate change and subject to intense investigations it can be expected that these numbers will be updated in future versions of the Climate Atlas.

5.2.4 The long term future

"Many changes due to past and future greenhouse gas emissions are irreversible for centuries to millennia, especially changes in the ocean, ice sheets and global sea level", IPCC AR6 said.

Beyond 2100, global sea level rise will continue to increase with high confidence primarily due to continued thermal expansion and loss of ice from both Greenland and Antarctic ice sheets including contributions from both surface melting and dynamical mass loss. Two critical issues need to be observed when looking beyond the year 2100. First, for Antarctica, the dynamical ice loss may include new instabilities such as the so-called Marine-Ice-Cliff-Instability [DeConto and Pollard, 2016], but our physical understanding is limited and confidence low for this contribution, as also reported in new studies [Edwards et al., 2019]. For continued high global mean temperatures in the range of 1-4°C, consistent with unchecked emissions (RCP8.5 and its Extended Concentration Pathways beyond 2100), the Greenland Ice sheet surface mass loss will be increasingly negative and a complete mass loss projected as a direct result over the next millennium or more. The exact path depends strongly on the emission scenario and there is medium confidence in the interval for the critical temperatures for irreversible and continued melt.

Neither AR5 nor SROCC addressed the past emissions-related sea level commitment. AR6 states that new evidence suggests that historical emissions up to 2016 will likely result in a committed sea level rise (i.e., the rise that would occur in the absence of additional emissions) of 0.7−1.1 m up to 2300, whereas emissions pledged through 2030 will likely increase the committed rise to 0.8−1.4 m [Fox-Kemper et al., 2021]. Since AR5, new knowledge of the Antarctic contribution in particular explains different estimates between AR5, SROCC and AR6. For RCP8.5, year 2300 the likely range of GMSL rise is 2.3-5.4 m in SROCC, while AR6 estimates GMSL will rise between 1.7 and 6.8 m by 2300 in the absence of MICI and by up to 16 m considering MICI, a wider range than AR5 and SROCC assessments. With a large Antarctic contribution, numbers corrected to the Danish Waters will be slightly higher. Considering the large and deep uncertainty this has not been pursued and no attempt is made to describe the regional differences due to land rise, which would generally be a negative local correction. DMI recommends to use the global estimates directly for Denmark, and to be prepared for updates of these multi-century numbers in the next years, as new knowledge appears.

5.2.5 Absolute and relative sea level rise

Absolute sea level describes the sea level in an "absolute reference frame", that is, a reference frame referring to the mass centre of the Earth. It is the quantity measured by satellite altimetry and calculated in climate models. Relative sea level describes the sea level relative to the coast or a reference system fixed on land, and thus includes the effects of land rise and subsidence. In the online Climate Atlas, relative sea level changes are available for all coastal stretches, including the regional land rise signal from DTU Space (see section 5.1.3). For local applications, it may be relevant to further correct for local subsidence or rise effects.

5.3 Results

Since the national Danish height system DVR90 is designed to give almost-zero mean sea level in year 1990, just a few years before the centre of our reference period, and the measured sea level may have a bias towards high sea level (Section 5.1.4), we used 0 cm, relative to DVR90, as mean sea level for the reference period. This introduces an error of maximum 8 centimetres, when analyzing the 14 tide gauge records in Hansen [2018].

With the method described above, the absolute sea level change is assumed to be the same for all coastal stretches in Denmark exposed to the open sea (Table 5). The median value for mean sea level rise is higher in the RCP8.5 scenario than in the RCP4.5 scenario, especially towards the end of the century, but with an overlap of the uncertainty intervals.

Table 5: Absolute mean sea level for Denmark [cm]. The values with brackets denote the best estimate and 10 to 90 percentile ranges, while the values for 2300 give the likely range.

	Present day 1981-2010	Mid century 2041-2070	End century 2071-2100	2300 likely range
RCP4.5		26 [7-45]	42 [10-74]	
RCP8.5	0	32 [8-57]	63 [19-108] 95-percentile 240	170 - 680

Relative sea level rise varies from one coastal stretch to the next. The relative sea level rise for individual coastal stretches can be viewed in the online Climate Atlas. Overall, the relative sea level changes are positive in all regions (the sea level is rising), with higher values towards the south and west, where the compensation from land rise is smaller. Except for this, the pattern is the same as for the absolute sea level.

6 Future extreme sea level events

6.1 Introduction

Changes in tides, storm surges, waves and other processes (e.g., coastal erosion, change of coastal ecosystems, salinization of soils, saltwater intrusion into ground and surface waters etc.) are superimposed on the slowly increasing mean sea level. Changes in, and interactions between, each of these processes can cause water level variability to become of even higher concern in the future. Understanding the combined future impact of these physical processes is a big challenge. This is especially true for the local scales considered in the Climate Atlas. The finer scale requires detailed knowledge of bathymetry, with high resolution, erosion processes and sedimentation, as well as wind fields with very high resolution in both time and space. Furthermore, the potentially increasing risk of compounding effects, such as storm surges and SLR, needs to be assessed. Therefore, a detailed hydrodynamical model has been developed and operated at DMI for operational storm surge modelling [Berg and Poulsen, 2012]. This model serves to provide sufficient details and knowledge for Climate Atlas, where the model is run with atmospheric forcing from climate models and uses the same high level of detail in coastline and bathymetry as in the operational model setup.

Extreme sea levels (ESLs) typically occur in association with storms [Pugh, 1987]. Such temporary raising of the water level originates from a combination of the wind stress acting on the sea surface and lowered air pressure (inverse barometer effect). Depending on the wind direction, the wind stress may generate ocean currents directed towards the shore. In shallow regions where the smaller water depth prevents a deeper return flow of water, the net shoreward transport can cause water to pile up along the coast, resulting in extreme water levels. The total still water level during the passage of storms also depends on the mean sea level and, in tidal regions, the timing of the tidal cycle. In the Western Baltic, further contributions to the water level can arise from pre-filling of the Baltic Sea and from standing waves (seiches) in the basins [Samuelsson and Stigebrandt, 1996].

In Denmark, water levels that exceed the 20-year return level (Section 4.2) are defined as storm surges by the Danish Storm Council. There is a large variation of local 20-year return levels, due to e.g. variable tidal range and wind conditions between different locations.

6.1.1 Storm surges today and usage for coastal planning – with caution

The present day storm surge statistics used for the reference period in the Climate Atlas are from the authoritative statistics, which are provided by the Kystdirektoratet (KDI, see Section 6.2). KDI provides the authoritative statistics reports for ESLs in Denmark, and is updated approximately every five years with the latest one published in 2017 and revised in 2019 [Ditlevsen et al., 2019]. The storm surge water statistics are based on measured water levels at tide gauge

stations along the Danish coasts (67 stations in the 2017 report) with a sufficiently long time-series. The 2017 statistics report, which is used for Climate Atlas, includes measurements until the beginning of 2017. For individual stations, different statistical methods are applied, giving an assessment of how frequently extreme water levels are to be expected.

A storm event can last for a short period of time or extend over several days. Several high water events can therefore be related to the same storm event. In this case, only the highest measured water levels recorded at the individual sites are treated as extreme water levels, and in order to ensure that the extreme water levels are independent a 36-hour criteria is applied. Such a principle is also adopted for climate simulations.

For the return levels not included in KDI statistics, we applied certain methods to extrapolate KDI statistics (discussed in Section 6.2). For coastal planning and climate adaptation, please note that these return levels under present climate should be used with caution, and should always be combined with an expert analysis of the local conditions. The major focus of the Climate Atlas project is to understand the influence of anthropogenic climate change and provide a dataset to support coastal climate adaptation strategy. There is little evidence that storm changes influencing Denmark (extratropical cyclones) in the past could be attributed to anthropogenic climate change (see the detailed discussion in Oppenheimer et al. [2019]). Therefore, the implementation of the KDI statistics for coastal planning today should remain. The following sections will discuss how we consider storm surge statistics under future climate change scenarios.

6.1.2   10.000 year storm surges return levels – under research

In order to develop cost-effective coastal defenses, an accurate calculation of the storm surge occurring once per 10000 years is required. The demand for an accurate assessment of the storm surge from the 10 000-year storm in Denmark's coastal towns is quite strong in the context of climate strategy planning along the coast. A more precise estimate, on the other hand, necessitates a greater number of observations. DMI is conducting a large number of research projects to reconstruct historical high storm surge episodes along the Danish coasts during the last 400 years. The reconstructions are based on artworks such as paintings, sketches, written documents, newspapers, and stories that have recently appeared in publications. The storm-surge levels of these storms have been estimated using numerical modelling of the coastal processes. Those reconstructions can be used in combination with extreme value statistics to give a more confident estimate of low probability events.

So far, the main challenge acknowledged broadly by experts in the field is that the data basis for the assessment is not adequate, and furthermore there is no consensus among experts on either the data basis or the method used to do it. As a result, the previously anticipated update of 10000 year storm surge indexes for all the coastal stretches have not been released in December 2021, as initially planned. For the time being, we recommend that users make use of the new information from the NCKF [Jacobsen et al., 2021] regarding the biggest storm surge incidents in historical records. We have also compared the data between release 2020b

and Jacobsen et al. [2021], and decided to take the data in coastal stretch OJ7 out compared to the release v2020b (see Section 6.2.1).

6.1.3 Why will storm surge heights increase?

Flood risk is exacerbated due to its interaction with the SLR. In Church et al. [2013b], ESL increase with SLR was marked as *very likely*. However, it was noted as *low confidence* in region-specific projections, as there was limited number of studies and a poor geographical coverage before the publication of AR5.

Since then, many datasets have become available, e.g. the Global Extreme Sea Level Analysis [GESLA-2 Woodworth et al., 2016]. Oppenheimer et al. [2019] concluded with *high confidence* that the inclusion of local processes is essential to estimate local changes in ESL. Thus, a thorough analysis of the local impact of winter storms is a prerequisite for a reliable local storm losses trend (the storm losses refer to the heavy damage of infrastructure and environment, restriction to traffic and injury or even loss of lives) [Donat et al., 2010].

Donat et al. [2011] investigated multi-model simulations from global (GCM) and regional (RCM) climate models, and found that extreme wind speeds will increase by up to 5% over northern parts of Europe in most simulations. We also made some investigations for several stations in Denmark using EURO-CORDEX members (see Section 6.2.2). It is hard to draw any conclusion from the current investigation, and further studies are necessary and planned for the next releases of the Climate Atlas.

6.1.4 Scope

The 2019 release of the Climate Atlas focuses on ESL events with statistical return periods (Section 4.2) of 20 and 50 years. Return periods have an inverse relationship to the average frequency of occurrence. Therefore, water levels corresponding to the 20 and 50 year return levels have a respective probability of 0.05 and 0.02 of being exceeded in any given year.

The 2020b release of the Climate Atlas focuses on the estimation of extreme water levels with a lower probability of occurrence, i.e. 100 and 10000 year return levels. In addition, return levels of 1 year and 5 year events are also estimated, as well as the future frequency of current 20 year events. The methods are partly illustrated in Figure 12, with more details in Section 6.2

The 2021b release of the Climate Atlas focuses on the estimation of the 'gate indexes'. 'Gate indexes' include the frequency and duration of the storm surges exceeding the current local warning levels. The current local warning levels are the storm surge warning levels for each municipalities used in Oct 2020 (Table 6).

6.1.5 Hydrodynamic modelling for extreme sea level studies

The ESL intensity change in the future can be estimated with statistical models or hydrodynamical models. The advantage of using hydrodynamical models is that they can quantify
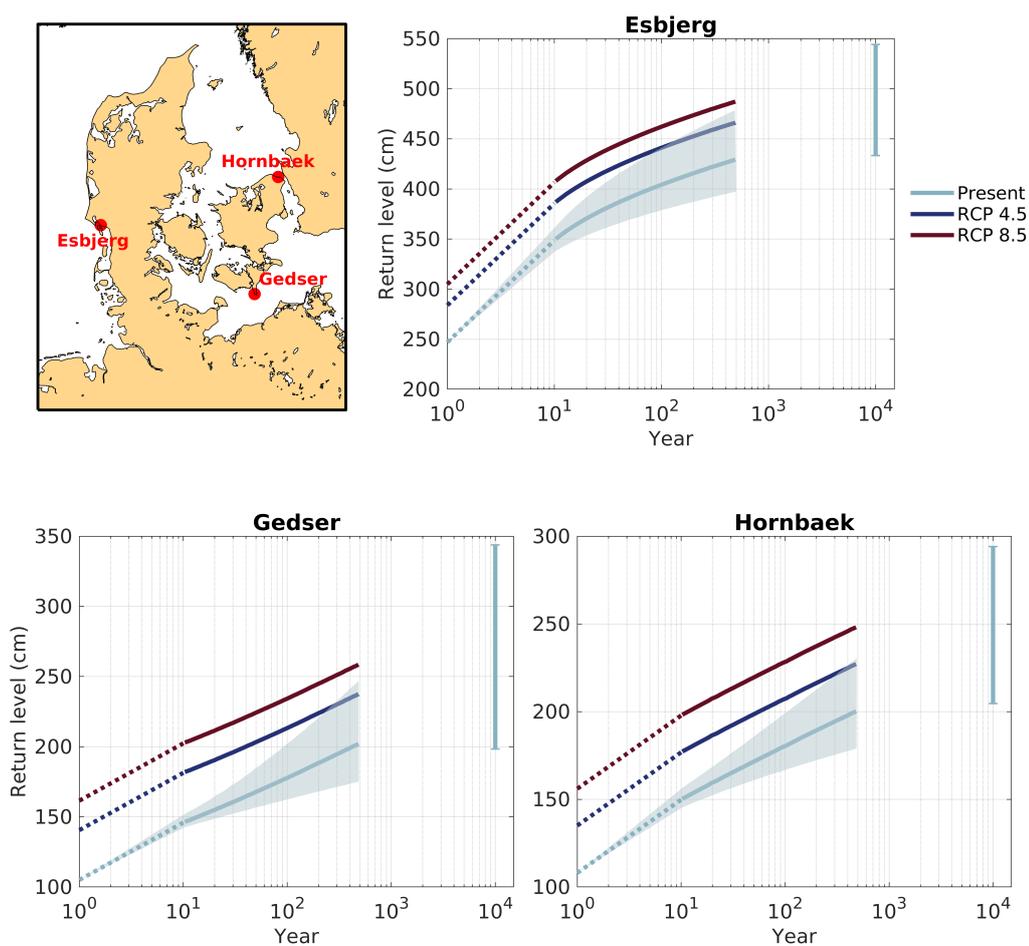
Figure 12: The expected extreme sea level (ESL, cm) at the end of this century with the corresponding return period on x-axis at the locations of the three oldest tide gauge stations in Denmark (locations are marked in the upper-left panel). The plots are comparing the present day values (grey) and the future conditions (RCP4.5 and RCP8.5 scenarios, in blue and red, respectively). The grey solid lines are based on tide gauge observations, and the grey bands refer to the 5−95% uncertainty range in the fit of the extreme value distribution to observations from Ditlevsen et al. [2019]. The dashed lines refer to the linear interpolation of the logarithmic return-time between 1 year and 10 year events. The error-bars indicate the uncertainty range for the extrapolated 10,000 year events under present climate.

interactions between the different components of ESL [Arns et al., 2013]. The important meteorological input for ocean models are wind speed and direction, and sea level pressure. From a global reanalysis data-set, modelled and observed sea level agreed quite well (with RMSE $<$ 0.2 m) over the reference period 1980-2011 [Muis et al., 2016]. However, it is still a challenge when running these models in climate mode because of inherent limitations of the climate projection data, e.g. resolution, precision and accuracy.

6.1.6 Challenges of sampling

The Climate Atlas model simulations are divided into time slices of 30 years. We use extreme value analysis (Section 4.2) to estimate the probability of events which occur on average less often than once within this period. The estimations are based on an implicit assumption of stationary statistics. Since each extreme events have a low probability of occurrence in any given year, but are here assumed independent, it is possible for several low probability events to appear by chance within a 30 year time slice. Occurrences of low probability events within this period will bias the return period towards low values. On the other hand, absence of low and moderately low probability events will result in a bias towards higher return periods. This sensitivity to the sampling period can be reduced by increasing the length of the sampling period, but this is a trade-off, since climatic stationarity in the sampling period is implicitly assumed.

6.1.7 Gate indexes and climate adaptation strategy

Storm surge gates (also known as flood barriers) are permanent structures that allow water to flow normally but have gates or bulkheads that can be closed during storm surges or spring tides to prevent flooding. They have the ability to seal the sea mouth of a river or waterway. Storm surge gates are designed to protect urban areas and infrastructure against storm surges and floods from the sea, and are planned for several urban areas in Denmark, including Copenhagen's harbor. The 'gate indexes,' which measure the frequency and duration of storm surges surpassing specific sea levels, were created for this purpose (gates). In this case, the 'storm surge gates' represent the current local warning levels.

In 2015, Denmark introduced national-level regulations for municipalities to develop climate adaptation plans, and as a result, some municipalities have requested DMI to offer warnings based on their own estimates, known as local warning levels (Table 6). When the emergency departments of the municipalities detect a potential concern, the local warning levels alter. We assessed the frequency and length of storm surges in the future using the same local warning levels as today in release 2021a.

6.2 Methods

6.2.1 Budget of storm surge changes

The climate historical simulation should be bias-corrected to the observations. For the uncoupled ocean simulations, one could apply the bias correction for the atmospheric forcing using adjust-mean methods. The adjust-mean methods allow to keep the variability of the climate model, while the climatology is adjusted to the observations. However, it is inappropriate to bias-correct the wind direction and pressure system [Mathis et al., 2013]. Hence, for the storm surge study, we have not seen bias-correction for the forcing as an appropriate way.

In Climate Atlas, we applied the 'delta change' method (Section 2.2) for the estimation of future storm surges. This means that we use observations for the present day values directly instead of bias correcting the model results. The future change of the storm surge statistics is directly added to the observed statistics. Another argument for the benefit of this method is that it facilitates the use of the KDI statistics. The KDI statistics should be kept since it is the authoritative storm surge statistics based on long-term observations, and to minimise the effect of the sampling problem mentioned in the last section.

However, for Climate Atlas release 2020b and v2021a, KDI statistics ("Højvandsstatistikker 2017") did not provide the 1, 5 and 10.000 year return levels. Thus we applied interpolation/extrapolation methods to the KDI statistics as shown in Figure 12. KDI statistics 2012 [Sørensen et al., 2013] provided 1 year return levels, which are directly used after evaluation. Thus, 5 year events are interpolated using 1 year and 10 year return levels. For 10000 year return levels, considering the large uncertainty for stations with observational records of less than 100 years, we only release data for the coastal stretches containing the 10 stations with records longer than 100 years in Climate Atlas (for record lengths, see Table 6). For those 10 stations, we applied a linear extrapolation method of the logarithmic return-time. Moreover, further evaluation of the estimated 10000 year event is conducted based on other datasets, including statistical methods different from the KDI statistics, hindcast model simulation results and model-based artificial extreme wind experiments.

In release v2021a, we retain ten stations for 10000 year return levels after comparing the data in release 2020b and with Jacobsen et al. [2021]. We applied the criterion that the measured maximum storm surge should fall within the uncertainty range. OJ7 (Lillebælt central) data is taken out since it does not meet the criteria. The other stations are subject to research and will be updated in a future release.

The algorithm for calculating storm surge change is described in section 8.2.3.

6.2.2 Simulations of wind-generated component

As described in Section 5.2.1, we employed a limited number of EURO-CORDEX members for the storm surge modelling in the Danish Climate Atlas project. The extreme wind from different RCMs differ from member to member and place to place. To provide a general picture of how the extreme wind in these two members differ from ensembles, we illustrated the time series of annual maximum wind speeds (AMWS) at two representative stations (Esbjerg and Hornbæk,

Figure 13). At Esbjerg station, the AMWS in HIRHAM5 showed about $10\,\mathrm{m\,s^{-1}}$ higher than ensemble, while the AMWS in RCA4 was closer to ensemble median values. We can draw very similar conclusions for the AMWS time-series at Hornbæk station. This investigation focuses on annual max wind speed only, whereas studies of storm tracks and related changes in wind direction and duration are left for the future.

6.2.3 Statistic methods for wind-generated component

To keep the consistency with other indexes in this report, we used POT and GPD methods to generate the storm surge return values (same parameterized extreme-value procedure is used as that described in Section 4). In POT methods, 30 events over the 30 year period were used as the threshold. However, there are two notable differences with other indexes in the current release. First, we are using the KDI statistics for the present day climate simulations, so the return value fitting methods for present day follow the definition from KDI (see 6.2). Second, for the uncertainty estimates, one assumption has to be made since we only used two ensemble members, i.e. the difference between two ensemble members should be smaller than the uncertainty range estimated by KDI present day statistics to guarantee the exclusion of the outliers.

To combine the uncertainty of storm surge and SLR, root squared methods are applied. However, for the rare storm surge events in release 2020b, we only consider the uncertainty of SLR for 100 year and 10000 year events, since 30 years slice is too short to estimate the low probability extreme storm surges. We further ensure that the e.g. 100 year return values are larger than 50 year return values and that they in-turn are larger than 20 year return values for both 10- and 90 percentiles.

6.3 Results

The extreme water level is an exceptional high water level, which occurs rarely and is caused by special wind and weather conditions. Depending on the locations, a big difference is expected when a water level can be characterised as an extreme. In Denmark, the biggest variation is found in the Danish part of the Wadden Sea, where extreme water levels can reach between 4 and 5.5 meters. Along the Kattegat coasts, extreme water levels over 2 meter are rare. Extraordinarily high water levels occurred as a result of strong storm wind and characteristic patterns of low and high pressure systems over Northern Europe, e.g. during Bodil storm Dec 2013. Such a strong storm event can also influence part of the Danish Straits (Danish: Bælterne), while the stations along the southern Baltic Sea coast are more influenced by Baltic type of storm.

With the methods described above, the best estimates of changes in 20-, 50-, 100- and 10000-year storm surges follow those of the mean sea level (see Section 5.3). The uncertainty range varies from one coastal stretch to the next, and depends on both the uncertainty of the
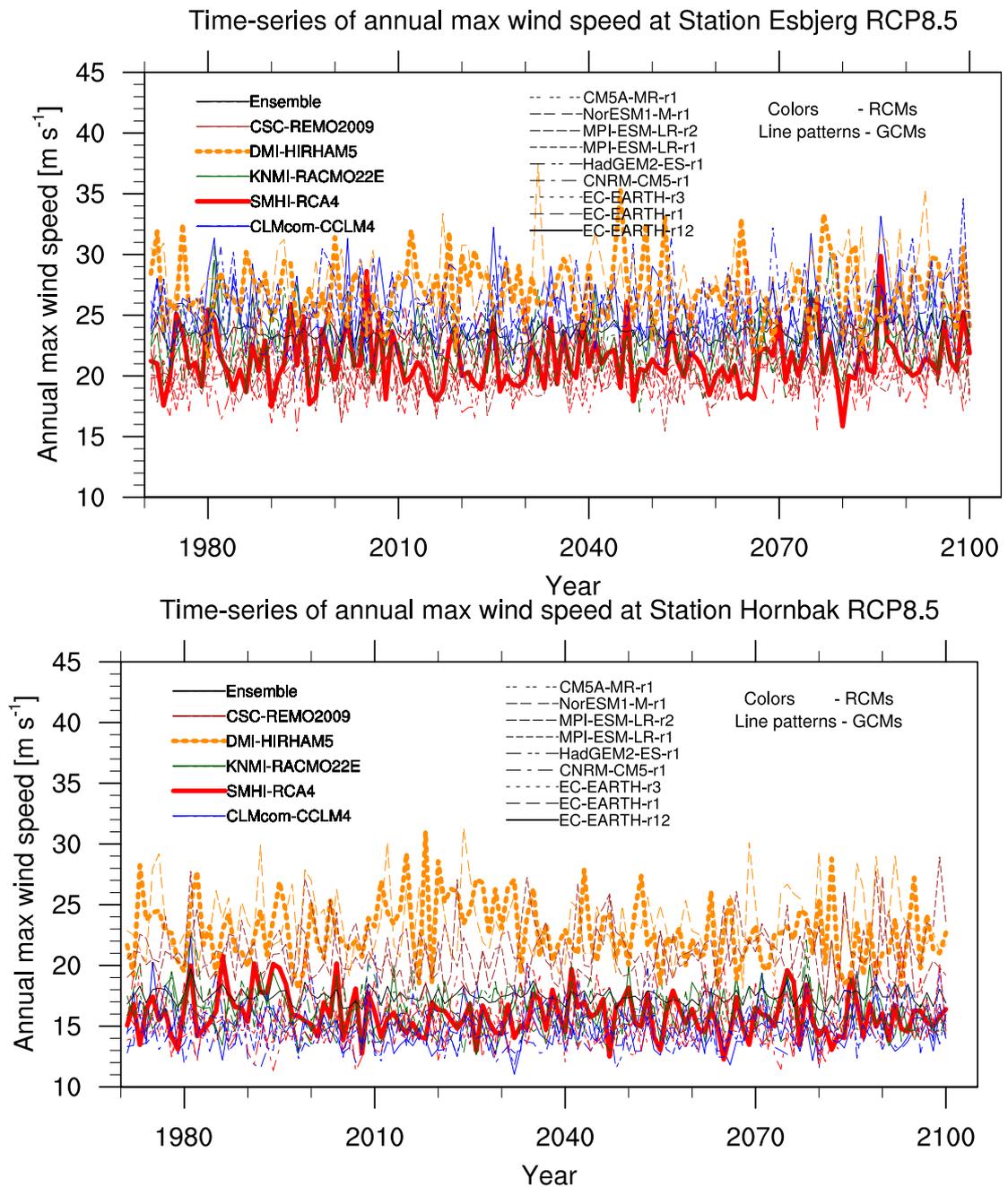
Figure 13: Time series of annual maximum wind speed (m s^{-1}) at the station Esbjerg (upper panel) and Hornbæk (lower panel). The time series are 130 years results from multi-RCM (16 members, including 5 RCMs: REMO2009 with 2, HIRHAM5 with 2, RACMO22E with 3, RCA4 with 5 and CCLM with 4 members) simulations under RCP 8.5 scenarios. The line colours indicate different RCMs, while different line patterns refer to GCMs (downscale to RCMs). DMI-HIRHAM5 and SMHI-RCA4 used in the current release are single dashed thick yellow line and thick red line respectively.

observation-based present day statistics, the hydrodynamic model simulations and the mean sea level rise uncertainty. All values are available in the online Climate Atlas.

7   Uncertainties

A data-product like the Climate Atlas should not only give the magnitudes of numerical quantities, but also the *uncertainties* coupled to these quantities.

Cloudbursts, for instance, are likely under-observed since the events are small in extent and rare. Limited lengths of records have their main impacts through sampling of the climate-variability: The climate system affecting Denmark has low-frequency variability and sampling such a sequence of data with limited-length windows causes a sampling issue: we may have samples from the real climate that are not representative of the mean climate. For instance, the North Atlantic Oscillation is a phenomenon influencing the track of low pressure systems in the North Atlantic. Therefore, temperatures, precipitation and winds over Denmark are dependent on the state of the NAO index. The influence of this is sampled by the limited availability of calibration-data.

At the moment, our understanding of the uncertainties is based on the spread provided by the models which we have available. Additional sources of uncertainty follow from the use of scope-limited observational material and from the use of interpolations and gridding techniques.

A good way to probe the relative importances of these sources of uncertainty, is to apply resampling of the data used, and re-parametrizations of the methods used. In 2019 we have employed resampling of observational data and the models used; in the future we will also probe the dependency on methods.

To perform the resampling of data we employ 'bootstrapping with replacement'. We apply the method to the years for which observational data exist, and for the models used. We do it separately so that the effects of these two important factors can be isolated.

The procedure is straightforward and is mainly one of repeating the calculation of the climate atlas indices under random picks of years or models, followed by collation of results. We simply look at the spread - standard deviation - in the main result we report on: the 10, 50 and 90%-iles themselves. We report results for the end-of century period and for the RCP8.5 scenario, as we expect the largest effects there.

In Table 10 we show the standard deviations of the percentile levels reported on in this report (i.e. 10, 50 and 90). We are sampling local anomalies in order to exclude the considerable effect of goegraphic variations.

The Table is complex to interpret quickly and we have put it at the end of this report so that unwarranted confusion does not arise upon encountering the table in the main text. A brief explanation of what is in the table follows, *but the reader mainly interested in following the flow of the text may wish to skip the rest of this paragraph*: For each index, and for either bootstrapping observations (label S1 at head of column) or models (header S2 on column) we give 4 numbers — these are on two lines and each pair is separated by a semi-colon. On the *first line* and *in front* of the semi-colon is given the largest (i.e. 'worst-case') standard deviation of any of the percentiles 10, 50 and 90 for absolute values in the climate index. On the first line

after the semi-colon is the largest standard deviation for any of the 10, 50 and 90%-iles of the *change* in the index. On the *second line* is given the same information as in the first line but now *only for the median* (i.e. the 50%-ile). We split the results in this way with the expectation that the effect on percentiles might not be the same for the 10, 50 and 90%-iles given small number statistics.

We did not apply bootstrapping on the climate indexes dealing with sea-levels and storm surges as the uncertainties there are given by error-propagating due to the limited number of sea level models currently available. In the future we could also probe the ocean-indices' uncertainties by resampling means.

So far, only 9 bootstraps have been performed, and only partially on factors S1 and S2. However, these first results allow some general conclusions.

We see some differences in the effects of bootstrapping S1 (observation years) and S2 (models), respectively: For index 001 and 106, the effects due to bootstrapping on S1 and S2 are about the same for the absolute values and the climate signals in these (i.e. their changes over time). For indices 101-105 the standard deviation in the climate change signal is much bigger for S2 bootstrapping than it is for S1 bootstrapping.

For indices 107 and 151-162 we only have results for S2 bootstrapping. Here we note that the standard deviation on the climate signal for 151-162, due to S2 bootstrapping, is in the range 5-16%.

107 has very small response to bootstrapping, it appears.

Only minor differences are seen throughout when comparing standard deviations induced by bootstrapping for any of the percentiles 10, 50 and 90 when just considering the 50th percentile.

In **summary**:

- choice of models has greater influence than the choice of calibration period, by factors of from 4 to 10 (indices 101-105)

- uncertainties due to model choice can reach 16% in the change of indices related to extreme precipitation

- robustness of the 10, 50 and 90th percentiles to S1 (observation years) and S2 (models) bootstrapping are similar.

We should thus seek to extend the number of models used, and we should accommodate an analysis of the importance of calibration period position in time which could not be sampled by the present bootstrap analysis. More and longer observed data series should be obtained.

Extending the number of factors considered in bootstrapping could provide us with an important tool for calculating 'total uncertainty' on the climate atlas information.

7.1   RCP4.5 error bars

The number of RCP4.5 models is about a factor of 2.5 less than for RCP8.5 and this leads to unfortunate effects due to small sample size and model inter-correlations (the few mod-

els present are somewhat dependent). The error bars for RCP4.5 results therefore show a tendency to vary a lot between future time periods, as well as, now and then, having unrealistically small widths. This prompts us to apply an adjustment scheme so that we can present estimated error bars for RCP4.5 results that are realistic.

We ensure that

1. The RCP4.5 error bars in near future and mid-century are adjusted so that the smaller one is scaled to the width of the larger one, and

2. the end of century error bar is scaled so that it is never the smallest of the three error bars.

The scaling algorithm applies a factor on the error bars, when scaling is called for, which retains the ratio of the upper (50 to 90 percentile interval) error bar to that of the lower (10 to 50 percentile) error bar, while keeping the median value fixed.

A larger ensemble of models would remedy this problem from the root, but the EURO-CORDEX ensemble of models is limited in scope for the RCP4.5 scenario.

8 Implementation details

8.1 Land areas - municipalities and main catchment areas

The detailed implementation of the calculation of each index is given in the following.

For each index calculations proceed as follows: Annual and seasonal mean (or also max/min, depending on the nature of the index) values are calculated at each EUR-11 grid-point from daily-mean model values. This gives 30 annual values for each of the chosen reference (historical and scenario) periods we have chosen. The mean of the 30 values is then taken. Then differences between historical and future periods are calculated for indices requiring relative changes. Then re-gridding and smoothing is applied to relative changes and absolute values to attain a smooth 1x1 km grid. 10, 50 and 90 percentile values are determined from these values.

8.1.1 Models used

The models we use from the CORDEX archive is a subsample of what is available. Not all of the CORDEX models are comparable: CNRM version 1 models used the incorrect boundary forcing and were excluded. Despite using a differently rotated grid, the Aladin model has been re-gridded to the EUR-11 standard grid, and is used. Table 7 and 8 list the models actually used.

8.1.2 Grid transformations

Interpolation is performed linearly to render the index values onto a 1x1 km grid ('det Danske Kvadratnet') from the EUR-11 grid of the models. The interpolation uses **Matlab** routine *scatteredInterpolant* which uses a Voronoi triangulation of the scattered sample points to perform interpolation. Natural neighbour interpolation is used via the "natural" option [Sibson, 1981]. Further implementation details for the *scatteredInterpolant* routine is given at Mathworks [2019].

8.1.3 Smoothing

Smoothing of the resulting 1x1 km grid is performed to avoid unrealistic details. We smooth all fields, after interpolation, by taking averages over moving box-windows of size 25×25 km. Since observed spatial structure is more credible than modelled future spatial structures in changes, we smooth the projections spatially with a bigger (75x75 km) filter, before calculating index changes (exception for winds, see Section 8.3).

Details on *det Danske KvadratNet* are available at Danmarks Statistik [2019].

For each index relative as well as absolute values of the expected values of the period-mean quantities are calculated. For relative changes we use the historical reference period

1981-2010, and the future periods 2011-2040, 2041-2070 and 2071-2100. These future periods are also used when giving the absolute values. The 10, 50 and 90 percentiles are calculated from the differences between the mean values over reference vs. scenario periods for each available model. The percentiles thus illustrate *model-spread*.

The boundaries for municipalities are defined by Styrelsen for Dataforsyning og Effektivisering (SDFE) and as this product can be updated we state here that the information was downloaded in May of 2018. Future updates by SDFE are bound to be have very minor impacts and are typically incremental when, typically, water-bodies (streams) and beach-lines change. See SDFE [2019].

The boundaries for main catchment areas are given by Miljøstyrelsen [MST, 2019].

The boundaries used for coastal stretches are discussed below in section 8.2.

8.1.4   Generic procedures

We next describe generic procedures for calculating area-specific absolute or relative-change indices for the temperature-like quantities in the atlas (index 001), the precipitation indices (101-106, 108-109, 151-162) and the cloudburst index (107). We will refer to these procedures when describing each index and note any deviations from the procedure, for completeness sake. Generic Procedure 1 deals with index 001 and 101-106. Generic procedure 2 deals with 151-162 and 201-203, and Generic Procedure 3 deals with index 107. Procedure 4 deals with some particular issues that arise in dealing with model temperatures.

8.1.4.1   Generic Procedure 1: For means and not very extreme indices

The following is the procedure specifically for temperature in land-areas such as municipalities and catchment areas, and the precipitation indexes.

1. Regridding of observational data to the CORDEX grid

   For all model grid points with at least 50% land coverage the nearest KGDK grid-point is found, and this 'nearest neighbour' time series is used as the assigned observational data point for that model grid point. We use nearest neighbour method, rather than interpolation, to avoid any smoothing of data implicit in most interpolation methods. Distance is calculated in the straight line - no great-circle calculation is performed. We determine whether the model grid cell has at least 50% land by inspecting the same grid-cell in the model land-sea mask. To ensure that small islands, for which the land-sea mask may indicate less than 50%, we specifically assign ls-mask values above 50% so that the data at the island have appropriate weight. This was done for Anholt and Læsø.

2. Bias Adjustment

   For each model, and for each of the 4+1 seasons, the 99 separate percentiles are determined for the observed data and for the model by interpolation in the assembled values. A robust linear regression is then performed using the 99 data-pairs, and the

slope of the regression line is noted. The slope is used to linearly extend the 99-point sequence beyond its range - to higher and lower values. See Figure 3 for an illustration of the procedure. The linear extensions are made starting in the last and first points of the sequence with the previously noted slope. On scenario data a quantile-quantile transformation is now performed using this constructed relationship. It is based on linear interpolation between points on the 99-pair percentile sequence if the interpoland (that is, the scenario value) is between the max and min of the sequence ordinate. If the interpoland falls either above or below the max and min of the ordinate range the linear extensions are used. The **matlab** robust regression routine is '*robustfit*'. When the 4 seasons have been completed, the results are combined to provide the annual time series.

3. Index calculation

   For each year, and each of the 4+1 seasons, and for each CORDEX model grid-point, in each model we calculate the index in question using the bias-adjusted data. Split the results into the 30-year long reference and future scenario periods (some models only have 29 years of data in the last of the future periods, and some end in November of the last year). Take means over the 30 values in each period, at each grid-point, and for each season etc. Calculate changes in indices (differences or ratios, in %, as appropriate, and noted for each index below) between the future periods in question and the reference period.

4. Regrid indices to the KGDK 1x1 km grid.

   Use the **matlab** routine '*scatteredInterpolant*' with option '*natural*'. This 'smooths the result' into neighbouring cells to a small degree. The 1x1 km land-sea mask is applied to remove apparent values over sea points.

   Smooth the observed results with **matlab** routine '*smooth2a*' using square 25x25 km windows - the window moves in 1-km steps; smooth projections for the future with 75x75 km windows.

5. Ensemble averaging

   For each 1x1 km grid-point collect the 68 model-index values relevant for the season and extract the 10, 50 and 90 percentiles, using the **matlab** routine named "*prctile*"[2], which *interpolates* in the values presented to it. This grid is one end-product for the homepage.

6. Area-aggregation

   For each municipality or main catchment area, identify the 1x1 km grid-points inside the boundary polygon - i.e. find all grid-points with centre-coordinate inside the given polygon. Calculate the mean of the 10, 50 and 90 percentile data generated above. This product is another product for the homepage.

---

[2]Used with implicit argument 'exact'.

8.1.4.2 Generic Procedure 2 - for extreme events   This procedure is used for rare precipitation events, except cloudbursts (see Generic Procedure 3 for that)

1. Recreation of Spildevandskommiteens NRM model (see [Gregersen et al., 2014b]). This results in a 10x10 km grid (on 'det Danske Kvadratnet') of the λ-parameter (number of exceedances of the threshold per year) and the scale-parameter for a generalized Pareto distribution. Both for 1-hour data and 24-hour data.

2. For the calibration-period and the reference as well as the three future periods, for land points only, for RCP4.5 and RCP8.5, we apply nearest-neighbour interpolation from the CORDEX model grid to the 10x10 km grid. The nearest-neighbour interpolation assigns the model series in the nearest CORDEX gridpoint to 'det Danske Kvadratnet' point under consideration.

3. Perform extreme value analysis for all models and the calibration period and all scenarios, and 1 and 24-hour data. 24-hour analysis performed with sliding windows covering 24-hours but advancing one hour each step).

    For lower and lower thresholds find model points exceeding the threshold until $\lambda = 3$ (events/year) is found (this will be a different threshold for each model, period and land-point, but all with $\lambda = 3$. Ensure at least 24 hours between each selected event.

    Fit a generalized Pareto distribution to the selected values, using the probability-weighted method. Thereby find local scale and shape parameters.

    Average the shape parameter to one national value.

    Calculate return-levels from the GP parameters for the calibration-period.

4. use the parameterized *q-q* transformation (see section 4) to correct the return-levels of the calibration period.

5. In the reference-period and the three future periods correct the return-levels using the parameterized *q-q* transformation determined in the calibration period (with Equation 5).

6. Files with *q-q* corrected return-values are prepared for the reference-period and the three future periods, for the next processing steps - i.e. Generic Procedure 1, steps 4-6.

8.1.4.3 Generic Procedure 3: cloudbursts   This procedure is used for cloudbursts but follows closely the method laid out for GP2, above. Since the models only have hourly data, and a cloudburst is defined as 'more than 15mm of precipitation in 30 minutes' we employ a simplified scaling method. From observations [Cappelen, 2017] we know that on a national observational system of about 258 measuring stations (numbers vary from year to year, the 258 average is for the 2011-2018 period), on average 87 cloudbursts were observed. That is, at each station on average you have to wait 3 years to observe a cloudburst.

1. Determine, in each gridpoint of each of the 1-hour precipitation models (see Table 8 for the complete list of model names) placed on 'det Danske Kvadratnet' grid, the event-level that occurs every three years.

2. For each model and each time period, use the relevant parameterized *q-q* transformation to convert the level determined in 1, to the return period.

3. Put gridded return periods into files for the next steps.

4. Finish with Generic Procedure steps 4-6.

8.1.4.4 Procedure 4: temperature maxima and minima and the daily temperature range

We discovered that the model-fields for temperatures, their maxima and their minima – which are delivered from CORDEX as separate files generated by the individual contributors – did not all fulfill such basic requirements as $T_{min} < T_{mean} < T_{max}$. So before starting the bias adjustment procedure for modelled daily minimum and maximum temperature, we made corrections for each model, each day and each grid cell so that T_{min} is given the lowest value of $T_{min}, T_{mean}, T_{max}$, and T_{max} is given the highest value of the three variables and T_{mean} is given the middle value of the three. The daily maximum and minimum temperatures were bias adjusted together rather than separately as with daily mean temperature using the steps below. The daily mean temperatures were QQ-scaled against gridded observed data from KGDK at a 20x20 km resolution for the period 1989-2019 using Procedure 2 already described.

- The modelled daily temperature range ($DTR = T_{max} - T_{min}$) was QQ-scaled against gridded observations for the period 2011-2019, resulting in DTR_{BA}. All instances were $DTR_{BA} < 0$ were set to 0.

- The skewness $Z = T_{mean} - (T_{max} + T_{min})/2$ was calculated for model data and then QQ-scaled against gridded observations, resulting in Z_{BA}.

- Then bias adjusted T_{min} and T_{max} were calculated using the equations $T_{min,BA} = T_{mean,BA} - Z_{BA} - DTR_{BA}/2$ and $T_{max,BA} = T_{mean,BA} - Z_{BA} + DTR_{BA}/2$.

The KGDK data for daily maximum and minmum temperatures used here is limited to the period 2011-2019. In 2011, a change in observing praxis occurs: before end of 2010 data were recorded from 6AM to next 6AM, but after start of 2011 it was recorded midnight to midnight. While T_{max} is very likely always recorded at a cadence of one day, we suspect that T_{min} may be recorded with occasionally unpredictable offsets of one day in the older system of recording because the coldest time of day is usually in the morning hours - sometimes before 6 AM, sometimes after - thus producing the larger variation in Z before end of 2010. This problem effectively limits us to use data after the start of 2011 for indexes involving bias-adjusted temperature maxima and minima. See Figure 14.
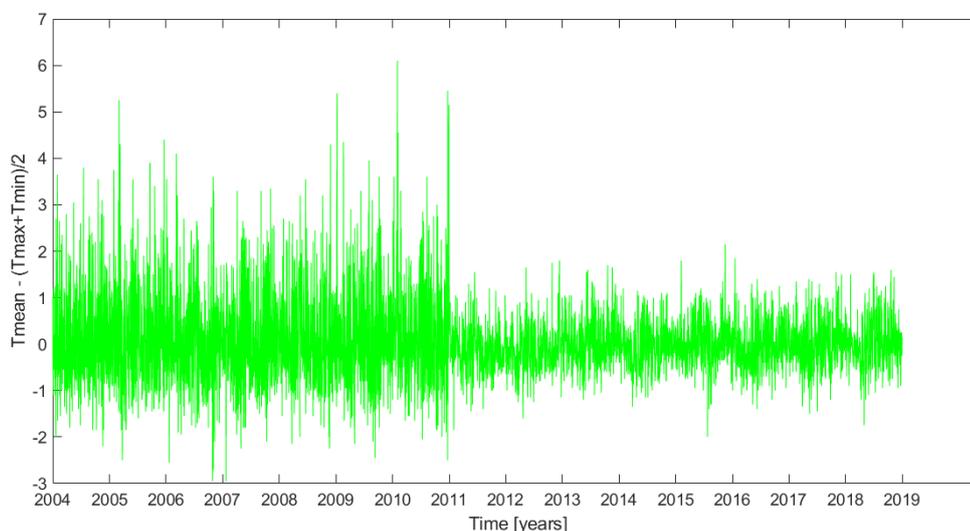
Figure 14: The skewness ($Z = T_{mean} - (T_{max} + T_{min})/2$) of 20x20 km gridded KGDK maximum and minimum temperature data changes at 2010/2011.

8.2   Implementation details for ocean indices

The detailed implementation of the calculation of ocean indices is given in the following.

8.2.1   Coastal stretches

The ocean indices are calculated for the 36 coastal stretches defined by Kystdirektoratet (KDI), except Ringkøbing Fjord and Nissum Fjord, which are regulated by lock gates (Table 6, KDI code VK2 and VK3). Each coastal stretch is represented by one station (Table 6), chosen to have the most reliable present day high water statistics for the coastal stretch. The mean sea level rise information and the hydrodynamic model results are interpolated to these stations using a nearest neighbour approach. Note that for 10 000 year extreme sea level indices, the length of the observed tide gauge time-series in some stations are too short to perform extreme value statistical analysis. Hence, these values are only included where the time series are sufficiently long (as described in Section 6.2).

The uncertainty intervals of the extreme sea level indices (202, 203) for the Limfjord (LF1, LF2, LF3 and LF4) have been calculated without expansion of the uncertainty interval based on hydrodynamic model simulations in the current *Klimaatlas*, since the hydrodynamic model for the Limfjord was not available for the study. They require separate simulations of a nested Limfjord model domain, which may be included in future updates.

8.2.2 Hydrodynamic model used

DMI operates the regional 3D ocean model HBM (the HIROMB-BOOS Model) for the North & Baltic Seas, in order to provide forecasts of the physical state of the Danish and nearby waters five days ahead [Berg and Poulsen, 2012, Fu et al., 2012]. We employed this operational model to perform the climate simulations. The DKSS operational setup (details on `http://ocean.dmi.dk/models/hbm.uk.php`) with the nested high-resolution inner Danish water domain was selected for the *Klimaatlas* project (model version HBM-2.8). The use of operational models for climate studies allow the same level of details in the climate projections as in the operational setup used for ocean forecast, and guarantees a well-tested and validated system. The validation of the storm surge forecast includes online validation and case studies can be found on `http://ocean.dmi.dk/validations/surges/index.uk.php`.

8.2.3 Implementation steps for storm surge indexes

1. Three CORDEX members was selected to perform the transient climate simulations (refer to Section 6.2.2).

2. We used the DMI storm surge operational model to derive the projected extreme sea levels (details in Sections 8.2.2 and 5.2.1).

3. Instead of bias-correcting the historical climate simulations, the KDI statistics were directly used for the present day/historical the storm surge indexes (Sections 6.2.1). Note that, obtaining 10000 year return levels requires extrapolation from the KDI statistics.

4. Using the two transient climate simulations to derive the uncertainties of the future storm surge change due to extreme wind change (Sections 6.2.3).

5. The uncertainties in SLR is root square added to the uncertainties of wind induced storm surge change. However, for 100 year and 10000 year return levels we only consider the uncertainties in SLR.

Table 6: The names of the 36 coastal stretches and the observing stations that represent the coastal stretches. The KDI code is the name of coastal stretch following the KDI definition. The local warning levels are listed in the second last column for estimating 'gate indexes'. The last column contains the records length for each tide gauge station in years.*VK2 Ringkøbing Fjord and VK3 Nissum Fjord are not included in *Klimaatlas*, as the water level in the two fjords are regulated by lock gates.

KDI code	Name for coastal stretch	Name for stations	Local warning levels (m)	Records length (y)
VH1	Vadehavskyst sydlig	Vidå	2.4	97
VH2	Vadehavskyst central	Ribe	2.4	97.6
VH3	Vadehavskyst nordlig	Esbjerg	2.0	143
VK1	Vestkyst central	Hvide Sande	1.9	30.7
VK2*	Ringkøbing Fjord	-	-	-
VK3*	Nissum Fjord	-	-	-
VK4	Vestkysten ud for Limfjorden	Thyborøn	1.9	46
VK5	Skagerrakkyst sydlige	Hanstholm	1.3	34.8
VK6	Skagerrakkyst nordlig	Hirtshals	1.3	47.2
LF1	Limford østlig	Nr. Sundby	1.3	51
LF2	Limfjorden ved Skive	Skive	1.3	21.3
LF3	Limfjorden ved Lemvig	Lemvig	1.3	53
LF4	Limfjorden ved Thisted	Thisted	1.3	15.3
OJ1	Kattegatkyst nordlige	Frederikshavn	0.9	122
OJ2	Ålborg Bugt	Hals Barre	1.3	45
OJ3	Randers Fjord og Mariager Fjord	Randers	1.25	105.1
OJ4	Djurslands østkyst og Anholt	Grenå	1.25	39.7
OJ5	Århus Bugt	Århus	1.25	128.3
OJ6	Lillebælt nordlig	Juelsminde	1.5	19.1
OJ7	Lillebælt central	Fredericia	0.84	127.4
SD1	Lillebælt sydlig	Fynshav	1.25	65.2
SD2	Sydfynske Øhav	Fåborg	1.0	15.6
SD3	Storebælt Sydvest	Slipshavn	0.9	126.8
SD4	Femern Bælt	Gedser	1.25	123.8
SD5	Smålandsfarvandet	Karrebæksminde	0.95	16
SD6	Falsters og Møns Østersøkyst	Hesnæs	1.25	23.8
SD7	Faxe Bugt	Rødvig	1.25	23.8
SJ1	Storebælt nordvest og Odense Fjord	Kerteminde	1.0	20.1
SJ2	Storebælt nordøst	Kalundborg	1.1	40.4
SJ3	Sejrø Bugt	Ballen	1.25	24.4
SJ4	Nordsjællands kyst	Hornbæk	1.1	125.8
SJ5	Isefjord	Holbæk	1.0	32.8
SJ6	Roskilde Fjord	Roskilde	0.9	21.8
SJ7	Øresunds kyst	København	1.4	127.9
SJ8	Køge Bugt	Køge	1.1	56.5
SJ9	Bornholms kyst	Tejn	1.25	24

8.3 Notes on Individual indices

The index numbers refer to Table 2.

- **001 Mean temperature** is entirely based on Generic Procedure 1. The complete list of CORDEX models used for this index are given in Tables 7 and. The observational data used to bias-adjust against, for this index, is taken from Klimagrid Danmark, with time coverage from 1989 to 2018, and with a spatial resolution of 20×20km. The time-resolution of this dataset is daily. The actual files accessed are given in Table 8. Two datasets are provided for Klimagrid Danmark - the first covers 1989-2010, and the other covers from 2011-2018.

- **002 Daily maximum temperature** The model data-set for daily maximum T is bias-corrected against Klimagrid Danmark gridded values. Daily KGDK data on the 20x20 km grid are used, covering the years 2011-2019.

- **003 Daily minimum temperature** The model data-set for daily minimum T is bias-corrected against Klimagrid Danmark gridded values. Daily KGDK data on the 20x20 km grid are used, covering the years 2011-19.

- **004 Highest temperature** The model values for seasonal/annual highest temperatures are bias-corrected using QQ-scaling against the KGDK observed values of that quantity, and the bias-corrected values averaged over the 30 years.

- **005 Lowest temperature** "Procedure 4" (a special procedure implemented to deal with specific model-related problems regarding temperature maxima and minima (See section 8.1.4.4 for details)

- **006 Annual temperature range** Generic Procedure 1.

- **007 Diurnal temperature range** Generic Procedure 4

- **008 Heat-wave days** Generic Procedure 4

- **009 Warm-wave days** Generic Procedure 4

- **010 Frost-days** Generic Procedure 4

- **011 Growing season length** Generic Procedure 1.

- **101 Mean precipitation** Like Generic Procedure 1 in section 8.1.4.1, but with these exceptions:

  1. Regridding, observational data based on the Klimagrid Danmark (KGDK) dataset with a spatial grid 10x10 km, and coverage is 1989-2018.

  2. Bias Adjustment, before application of the BA algorithm all zero values are set to a small random number between 0 and 10^{-12} in model and observations; after BA all adjusted model numbers smaller than 0.1 are set to zero.

3. Index calculation, the relative change in percent is calculated.

4 - 5 - 6. The same as in Generic Procedure 1.

- **102 Daily max precipitation.** Just like index 101 but the mean of the 30 annual maxima (or annual series of seasonal maxima) is taken.

- **103 5-day max precipitation.** A 5-day window is moved along the precipitation time-series and the sum over the 5 days calculated and noted against the centre day of the window. This means that 2 days at the start and 2 days at the end are lost. Then the maximum values of this series for the relevant 4+1 seasons etc are determined.

- **104 14-day max precipitation.** Just like index 103, but instead of a 2+1+2 day window a 6+1+7 day window is employed.

- **105 Days with more than 10 mm precipitation in a day.** A count is made of the number of days with more daily precipitation that 10mm, for the relevant 4+1 seasons, etc. That gives 30 annual counts which are averaged.

- **106 Days with more than 20 mm precipitation.** Just like index 105, but for 20 mm precipitation.

- **107 Number of cloudbursts.** The number of cloudbursts per year are derived from the parametrised EVD for future periods given the current rate of observed cloudbursts.

- **108 Number of dry days** Number of days of the year or season with precipitation below 1 mm.

- **109 Maximum dry spell length** Length of the longest period of the year or season with consecutive days with precipitation below 1 mm

- **110 Fraction of season or years that are dry** Fraction of seasons or years that would be considered the 5 driest during the reference period

- **112 Number of 5-day drought periods** Number of sequences at least 5 days long with less than 1mm precipitation per day.

- **115 Number of 10-day drought periods** Number of sequences at least 10 days long with less than 1mm precipitation per day.

- **152 hourly precipitation of events with 5-year return period (in mm/hr)** As index 151 above but for 5-year events.

- **153 hourly precipitation of events with 10-year return period (in mm/hr)** As index 151 above, but for 10-year events.

- **154 hourly precipitation of events with 20-year return period (in mm/hr)** As index 151 above, but for 20-year events.

- **155 hourly precipitation of events with 50-year return period (in mm/hr)** As index 151 above, but for 50-year events.

- **156 hourly precipitation of events with 100-year return period (in mm/hr)** As index 151 above, but for 100-year events.

- **157 24-hour total precipitation of events with 2-year return period (mm/day)**. As 151 but for 24-hour total precipitation sums. Sliding 24-hour windows, stepping at 1-hr resolution, are used.

- **158 24-hour total precipitation of events with 5-year return period (mm/day)** Sliding 24-hour windows, stepping at 1-hr resolution, are used.

- **159 24-hour total precipitation of events with 10-year return period (mm/day)**. Sliding 24-hour windows, stepping at 1-hr resolution, are used.

- **160 24-hour total precipitation of events with 20-year return period (mm/day)** Sliding 24-hour windows, stepping at 1-hr resolution, are used.

- **161 24-hour total precipitation of events with 50-year return period (mm/day)** Sliding 24-hour windows, stepping at 1-hr resolution, are used.

- **162 24-hour total precipitation of events with 100-year return period (mm/day)**. As 110 but for 24-hour total precipitation sums. Sliding 24-hour windows, stepping at 1-hr resolution, are used.

- **201 Mean sea level rise (cm)** has two components, i.e. IPCC based regional mean sea level rise and land uplift. The IPCC report provides the global mean sea level rise information, which was further downscaled to regional mean sea level rise for Denmark. The regional mean sea level rise is identical for the whole Denmark. The land uplift provides the difference for different coastal stretches.

- **202 Storm surge 20-year return events (cm)** is based on the 10 minutes sea level data from the HBM model output and observations.

- **203 Storm surge 50-year return events (cm)**. As 202 but for 50-year events.

- **204 Storm surge 100-year return events (cm)**. The historical period are based on KDI statistics and the future change only considers SLR.

- **205 Storm surge 10000-year return events (cm)**. As 204 but for 10000-year events.

- **206 Storm surge 1-year events (cm)**. As 202 but for 1-year events.

- **208 Storm surge 5-year events (cm)**. As 202 but for 5-year events.

- **210 Frequency of storm surge 20-year events (number of events per 20 years)**. For the historical periods, it is calculated as the observation records divided by the number of events over 20-year return level. For the future periods, it is calculated as the simulations time (30 years) divided by the number of events over the historical 20-year return level.

- **211 Frequency of storm surge events exceeding current local warning level (number of events per year)**. For the historical periods, it is calculated as the number of storm surge events exceeding the local warning levels at each station according to the hindcast simulation. This hindcast simulation is 1961 - 2018. For the future periods, it is calculated as the simulated storm surge events exceeding the current local warning levels in 30 years, divided by 30 years.

- **212 Accumulated duration of sea level exceeding current local warning level (hours per year)**. For the historical periods, it is calculated as the accumulated time of sea level exceeding the local warning levels at each station according to the hindcast simulation. This hindcast simulation is 1961 - 2018. For the future periods, it is calculated as the simulated sea level exceeding the current local warning levels in 30 years, divided by 30 years.

- **301 Mean wind speed (m/s)**. Wind speed is calculated for bias-corrected data using the QQ-scaling method and given as a mean over a year or a season. Because of large gradients in wind speed inland from the coasts, the smoothing is reduced compared to other indices: a 25 x 25 km filter is applied instead of the general 75 x 75 km filter.

- **302 Extreme wind (m/s)** calculated as the number of days for a year or season with a maximum wind speed above 25 m/s.

  Because of large gradients in wind speed inland from the coasts, the smoothing is reduced compared to other indices: a 25 x 25 km filter is applied instead of the general 75 x 75 km filter.

- **401 Solar radiation (W/m^2)** Also known as 'globalstråling' in Danish; the sum of direct and diffuse sunlight reaching the surface. The corresponding model field is *downwelling shortwave radiation at the surface*.

- **402 Potential evaporation (mm/day)** Calculated using the Makkink formula based on temperature and solar radiation for both model and observational data.

- **501 mean summer fire weather index** FWI based on Wang et al. [2015]. Mean over JJA.

- **502 'High' fire weather index days** Number of days with FWI > 18.5

- **503 'Extreme' fire weather index days** Number of days with FWI > 29.5

RCP8.5

	RCA	CCLM	crCLIM	REMO	RACMO	HIRHAM	WRF	ALADIN	RegCM	Total
MOHC-HadGEM2-ES	1	1	1	1	1	1	2	1	1	10
ICHEC-EC-EARTH	3	1	3	1	3	3	2		1	17
CNRM-CERFACS-CNRM-CM5			1	1	1	1	1	2	1	8
NCC-NorESM1-M	1		1	1	1	1	1		1	7
MPI-M-MPI-ESM-LR	3	1	3	3	1	1	1		1	14
IPSL-IPSL-CM5A-MR	1			1	1	1	1			5
CCCma-CanESM2		1		1						2
MIROC-MIROC5		1		1			1			3
Total	9	5	9	10	8	8	9	3	5	66

RCP4.5

	RCA	CCLM	crCLIM	REMO	RACMO	HIRHAM	WRF	ALADIN	RegCM	Total
MOHC-HadGEM2-ES	1	1		1	1	1				5
ICHEC-EC-EARTH	1	1		1	2	1				6
CNRM-CERFACS-CNRM-CM5					1			2		3
NCC-NorESM1-M	1			1		1				3
MPI-M-MPI-ESM-LR	1	1		2						4
IPSL-IPSL-CM5A-MR	1						1			2
Total	5	3		5	4	3	1	2		23

RCP2.6

	RCA	CCLM	crCLIM	REMO	RACMO	HIRHAM	WRF	ALADIN	RegCM	Total
MOHC-HadGEM2-ES	1	1		1	1	1				5
ICHEC-EC-EARTH	1	1		1	1	1				5
CNRM-CERFACS-CNRM-CM5				1	1			1		3
NCC-NorESM1-M	1			1	1				1	4
MPI-M-MPI-ESM-LR	1	2		2	1		1		1	8
IPSL-IPSL-CM5A-MR										
MIROC-MIROC5				1					1	2
Total	4	4		7	5	2	1	1	3	27

Table 7: RCP8.5 (top), RCP4.5 (middle) and RCP2.6 (bottom) EURO-CORDEX models used in producing the indexes 001, 101-106 and 108-109

RCP8.5

RCP8.5	RCA	CCLM	crCLIM	REMO	RACMO	HIRHAM	WRF	ALADIN	RegCM	Total
MOHC-HadGEM2-ES	1		1	1	1	1		1		6
ICHEC-EC-EARTH	3		3	1	1	3			1	12
CNRM-CERFACS-CNRM-CM5			1	1		1		1	1	5
NCC-NorESM1-M	1		1	1		1			1	5
MPI-M-MPI-ESM-LR	3	1	3	3		1			1	12
IPSL-IPSL-CM5A-MR	1			1		1				3
CCCma-CanESM2		1		1						2
MIROC-MIROC5		1		1						2
Total	9	3	9	10	2	8		2	4	47

RCP4.5

RCP4.5	RCA	CCLM	crCLIM	REMO	RACMO	HIRHAM	WRF	ALADIN	RegCM	Total
MOHC-HadGEM2-ES	1			1	1	1				4
ICHEC-EC-EARTH	1			1	1	1				4
CNRM-CERFACS-CNRM-CM5								1		1
NCC-NorESM1-M	1			1		1				3
MPI-M-MPI-ESM-LR	1			2						3
IPSL-IPSL-CM5A-MR	1									1
Total	5			5	2	3		1		16

RCP2.6

RCP2.6	RCA	CCLM	crCLIM	REMO	RACMO	HIRHAM	WRF	ALADIN	RegCM	Total
MOHC-HadGEM2-ES	1					1				2
ICHEC-EC-EARTH	1					1				2
CNRM-CERFACS-CNRM-CM5				1						1
NCC-NorESM1-M	1			1					1	3
MPI-M-MPI-ESM-LR	1								1	2
Total	4			2		2			2	10

Table 8: RCP8.5 (top), RCP4.5 (middle) and RCP2.6 (bottom) EURO-CORDEX models used in producing the indexes indexes 107, 151-162.

Table 9: Observational data used for the various climate indices. Data sources are labelled with numbers and are - **1:** Klimagrid Danmark (KGDK) from DMI database. A subset is available her: `https://www.dmi.dk/fileadmin/Rapporter/TR/tr12-10_20x20km.zip`. Note that KGDK precipitation data are not undercatch-corrected. - **2:** DMI database, Data-table on page 73 of Cappelen [2017] - **3:** Ditlevsen et al. [2019].

Number	Type of data	Source	Spatial res.	Time res.	Time coverage	Notes
001 - mean T	KGDK dataset	1	20×20km	Daily mean	1989–2019	Two files used, one for 1989-2000 and another for 2001-2019
002-005, 007-009	KGDK dataset	1	10x10 km	Daily mean	2011-2019	-
101-106, 108-110, 112, 115	KGDK dataset	1	10x10km	Daily mean	2004-2019	Daily files
107 - Cloudbursts	DMI hi-res precip network	2	≈ 258 stations	Minutes	2011-2016	Observed rate of cloudbursts/year/station given station network
201 - 203 Ocean	KDI-based parameters	3	Coastal	Hourly - 10 min.	20th C - Now.	We use KDI-derived extreme-value distribution parameters for each station.
301 Wind	KGDK dataset	1	20x20 km	Daily mean	1989–2019	Two files used, one for 1989-2000 and another for 2001-2019
302 Wind	KGDK dataset	1	10x10 km	Daily mean	2011-2019	-
401 Global rad.	KGDK dataset	1	20x20 km	Daily mean	1989–2019	Two files used, one for 1989-2000 and another for 2001-2019
402 Makkink evap.	KGDK dataset	1	20x20 km	Daily mean	1989–2019	Two files used, one for 1989-2000 and another for 2001-2019
501-503	KGDK dataset	1	10x10km	Daily mean, Hourly means	2011-2022	FWI calculated from KGDK observations

The Danish Meteorological Institute

Table 10: Standard deviations in climate indexes, based on bootstrapping of local anomaly data (i.e. excluding the enhanced variability otherwise due to inclusion of geographic variations). Observation year and models are bootstrapped – labelled S1 and S2. Two pieces of information is given for each index - one is the absolute value of an index in the far future period 2071-2100, and the other is the change in that index between the far future period and the historical reference period. These two quantities are shown in each column before and after the semi-colon. The changes are either absolute (indexes 001, 105, 106 and 107), or are given as percentages. Values shown are for the scenario RCP8.5 and the distributions generated by the bootstrap include the various values from each bootstrap across the whole 1x1 km land-only grid of Denmark. 9 bootstraps were performed. For each index two lines are shown - the first line gives the largest standard deviation found in any of the 10, 50 and 90%iles - the second line is restricted to just the 50%ile (i.e., the median). The seasonal and the annual values are all included, except for index 107, which is annual only.

#	Name of index	units	S1 (obs)	S2 (mod)
001	Mean temperature	$°C : °C$	$\pm0.18 : \pm0.13$ $\pm0.18 : \pm0.13$	$\pm0.16 : \pm0.17$ $\pm0.12 : \pm0.12$
101	Mean precip.	mm/day : %	$\pm0.13 : \pm1.0$ $\pm0.13 : \pm0.9$	$\pm0.12 : \pm5$ $\pm0.09 : \pm4$
102	Daily-max precip.	mm : %	$\pm1.7 : \pm0.6$ $\pm1.7 : \pm0.5$	$\pm1.6 : \pm6$ $\pm1.0 : \pm4$
103	5-day max precip.	mm : %	$\pm2.6 : \pm0.86$ $\pm2.5 : \pm0.74$	$\pm2.0 : \pm4$ $\pm1.5 : \pm3$
104	14-day max precip.	mm : %	$\pm3.9 : \pm0.9$ $\pm3.8 : \pm0.8$	$\pm4.5 : \pm5$ $\pm2.4 : \pm4$
105	Days with over 10 mm Daily precip.	days : days	$\pm0.7 : \pm0.15$ $\pm0.7 : \pm0.13$	$\pm0.55 : \pm0.57$ $\pm0.43 : \pm0.48$
106	Days with over 20 mm Daily precip.	days : days	$\pm0.35 : \pm0.12$ $\pm0.35 : \pm0.10$	$\pm0.20 : \pm0.20$ $\pm0.14 : \pm0.15$
107	Number of cloud-bursts per year	events : events	- -	$\pm0.074 : \pm0.073$ $\pm0.074 : \pm0.073$
151	Hourly precip. in 2-year events	mm : %	- -	$\pm0.90 : \pm7$ $\pm0.69 : \pm6$
153	Hourly precip. in 10-year events	mm : %	- -	$\pm3.0 : \pm10$ $\pm2.4 : \pm9$
156	Hourly precip. in 100-year events	mm : %	- -	$\pm8.6 : \pm16$ $\pm5.9 : \pm13$
157	Daily precip. in 2-year events	mm : %	- -	$\pm2.2 : \pm5.3$ $\pm1.7 : \pm4.3$
159	Daily precip. in 10-year events	mm : %	- -	$\pm4.9 : \pm7.8$ $\pm3.0 : \pm5.4$
162	Daily precip. in 100-year events	mm : %	- -	$\pm11.7 : \pm11.4$ $\pm5.8 : \pm6.1$
201	Mean sea level wrt. coastline		-	-
202	Storm surge 20-year events		-	-
203	Storm surge 50-year event		-	-

#	GCM	RCM	member	tas	tasmax	tasmin	pr	pr1h	sfcWind	sfcWindmax	rsds	hurs
1	CANESM	CCLM	r1i1p1	h8	h8	h8	h8	h8	h8		h8	h8
2	CANESM	REMO15	r1i1p1	h8	h8	h8	h8	h8	h8	h8	h8	
3	CNRM	crCLIM	r1i1p1	h8	h8	h8	h8	h8	h8	h8	h8	
4	CNRM	ALADIN	r1i1p1	h48	h48	h48	h48	h48	h48	h48	h48	
5	CNRM	HIRHAM	r1i1p1	h8	h8	h8	h8	h8	h8	h8	h8	h8
6	CNRM	REMO15	r1i1p1	h28	h28	h28	h28	h28	h28	h28	h28	h28
7	CNRM	REGCM	r1i1p1	h8	h8	h8	h8	h8	h8	h8	h8	
8	CNRM	WRF381	r1i1p1	h8	h8	h8	h8		h8	h8	h8	
9	CNRM	RACMO	r1i1p1	h248	h248	h248	h248		h248	h248	h248	h248
10	CNRM	HADREM	r1i1p1	h8	h8	h8	h8		h8	h8	h8	h8
11	ECEARTH	crCLIM	r1i1p1	h8	h8	h8	h8	h8	h8	h8	h8	h8
12	ECEARTH	HIRHAM	r1i1p1	h8	h8	h8	h8	h8	h8	h8	h8	h8
13	ECEARTH	RACMO	r1i1p1	h48	h48	h48	h48	h48	h48	h48	h48	h48
14	ECEARTH	RCA	r1i1p1	h8	h8	h8	h8	h8	h8	h8	h8	h8
15	ECEARTH	WRF361	r1i1p1	h8			h8				h8	
16	ECEARTH	crCLIM	r3i1p1	h8	h8	h8	h8	h8	h8	h8	h8	h8
17	ECEARTH	HIRHAM	r3i1p1	h248	h248	h248	h248	h248	h248	h248	h248	h248
18	ECEARTH	RACMO	r3i1p1	h8	h8	h8	h8		h8	h8	h8	h8
19	ECEARTH	RCA	r3i1p1	h8	h8	h8	h8	h8	h8	h8	h8	h8
20	ECEARTH	CCLM	r12i1p1	h248	h248	h248	h248		h248	h248	h248	
21	ECEARTH	crCLIM	r12i1p1	h8	h8	h8	h8	h8	h8	h8	h8	h8
22	ECEARTH	HIRHAM	r12i1p1	h8	h8	h8	h8	h8	h8	h8	h8	h8
23	ECEARTH	REMO15	r12i1p1	h248	h248	h248	h248	h48	h248	h248	h248	
24	ECEARTH	REGCM	r12i1p1	h8	h8	h8	h8	h8	h8	h8	h8	h8
25	ECEARTH	WRF381	r12i1p1	h8	h8	h8	h8		h8	h8	h8	h8
26	ECEARTH	RACMO	r12i1p1	h248	h248	h248	h248		h248	h248	h248	h248
27	ECEARTH	HADREM	r12i1p1	h28	h28	h28	h28	h28	h28	h28	h28	h28
28	ECEARTH	RCA	r12i1p1	h248	h248	h248	h248	h248	h248	h248	h248	h248
29	ECEARTH	WRF361	r12i1p1	h8	h8	h8	h8		h8			
30	HADGEM	CCLM	r1i1p1	h48	h48	h48	h48		h48	h48	h48	
31	HADGEM	crCLIM	r1i1p1	h8	h8	h8	h8	h8	h8	h8	h8	h8
32	HADGEM	ALADIN	r1i1p1	h8	h8	h8	h8	h8	h8	h8	h8	
33	HADGEM	HIRHAM	r1i1p1	h248	h248	h248	h248	h248	h248	h248	h248	h248
34	HADGEM	REMO15	r1i1p1	h248	h248	h248	h248	h48	h248	h248	h248	
35	HADGEM	REGCM	r1i1p1	h28	h28	h28	h28		h28	h28	h28	h28
36	HADGEM	WRF381	r1i1p1	h8	h8	h8	h8		h8	h8	h8	
37	HADGEM	HADREM	r1i1p1	h28	h28	h28	h28	h28	h28	h28	h28	h28
38	HADGEM	RACMO	r1i1p1	h248	h248	h248	h248	h48	h248	h248	h248	h248
39	HADGEM	RCA	r1i1p1	h248	h248	h248	h248	h248	h248	h248	h248	h248
40	HADGEM	WRF361	r1i1p1	h8	h8	h8	h8		h8		h8	
41	IPSL	HIRHAM	r1i1p1	h8	h8	h8	h8	h8	h8	h8	h8	h8
42	IPSL	REMO15	r1i1p1	h8	h8	h8	h8	h8	h8	h8	h8	h8
43	IPSL	WRF381	r1i1p1	h48	h48	h48	h48		h48	h48	h48	
44	IPSL	RACMO	r1i1p1	h8	h8	h8	h8		h8	h8	h8	h8
45	IPSL	RCA	r1i1p1	h48	h48	h48	h48	h48	h48	h48	h48	h48
46	MIROC	CCLM	r1i1p1	h28	h28	h28	h28	h8	h28		h28	h8
47	MIROC	REMO15	r1i1p1	h28	h28	h28	h28		h28	h28	h28	
48	MIROC	WRF361	r1i1p1	h8			h8		h8		h8	
49	MPI	CCLM	r1i1p1	h248	h248	h248	h248	h8	h248	h248	h248	
50	MPI	crCLIM	r1i1p1	h8	h8	h8	h8	h8	h8	h8	h8	h8
51	MPI	HIRHAM	r1i1p1	h8	h8	h8	h8	h8	h8	h8	h8	h8
52	MPI	REGCM	r1i1p1	h28	h28	h28	h28	h28	h28	h28	h28	h28
53	MPI	WRF381	r1i1p1	h8	h8	h8	h8		h8	h8	h8	h8
54	MPI	RACMO	r1i1p1	h28	h28	h28	h28		h28	h28	h28	h28
55	MPI	HADREM	r1i1p1	h8	h8	h8	h8	h8	h8	h8	h8	h8
56	MPI	REMO09	r1i1p1	h248	h248	h248	h248	h48	h248	h248	h248	
57	MPI	RCA	r1i1p1	h248	h248	h248	h248	h248	h248	h248	h248	h248
58	MPI	WRF361	r1i1p1	h28	h28	h28	h28		h28		h28	
59	MPI	crCLIM	r2i1p1	h8	h8	h8	h8	h8	h8	h8	h8	h8
60	MPI	REMO09	r2i1p1	h248	h248	h248	h248	h48	h248	h248	h248	
61	MPI	RCA	r2i1p1	h8	h8	h8	h8	h8	h8	h8	h8	
62	MPI	crCLIM	r3i1p1	h8	h8	h8	h8	h8	h8	h8	h8	h8
63	MPI	REMO15	r3i1p1	h8	h8	h8	h8	h8	h8	h8	h8	h8
64	MPI	RCA	r3i1p1	h8	h8	h8	h8	h8	h8	h8	h8	h8
65	NORESM	crCLIM	r1i1p1	h8	h8	h8	h8	h8	h8	h8	h8	h8
66	NORESM	HIRHAM	r1i1p1	h48	h48	h48	h48	h48	h48	h48	h48	h48
67	NORESM	REMO15	r1i1p1	h248	h248	h248	h248	h248	h248	h248	h248	h248
68	NORESM	REGCM	r1i1p1	h28	h28	h28	h28	h28	h28	h28	h28	h28
69	NORESM	WRF381	r1i1p1	h8	h8	h8	h8		h8	h8	h8	
70	NORESM	HADREM	r1i1p1	h8	h8	h8	h8	h8	h8	h8	h8	
71	NORESM	RACMO	r1i1p1	h28	h28	h28	h28		h28	h28	h28	h28
72	NORESM	RCA	r1i1p1	h248	h248	h248	h248	h248	h248	h248	h248	h248

Figure 15: List of the 72 climate model simulations used for the v2024a climate indices produced within *Klimaatlas*. Each row represents one model simulation with a forcing global climate model (GCM) and a downscaling regional climate model (RCM) and a member identification in the case when several downscalings are available. Columns represent one variable used: tas (daily mean temperature), tasmax (daily maximum temperature), tasmin (daily minimum temperature), pr (daily total precipitation amount), pr1h (hourly total precipitation amount), sfcWind (daily mean wind speed), sfcWindmax (daily maximum wind speed), rsds (daily mean down-ward shortwave radiation) and hurs (relative humidity). For each variable and model simulation we denote the scenarios available by h (historical period), 2 (RCP2.6), 4 (RCP4.5) and 8 (RCP8.5).

References

A. Arns, T. Wahl, I.D. Haigh, J. Jensen, and C. Pattiaratchi. Estimating extreme water level probabilities: A comparison of the direct methods and recommendations for best practise. *Coastal Engineering*, 81:51–66, November 2013. doi: $10.1016/\text{j.coastaleng.}2013.07.003$. URL `https://doi.org/10.1016/j.coastaleng.2013.07.003`.

Jonathan L Bamber, Richard M Westaway, Ben Marzeion, and Bert Wouters. The land ice contribution to sea level during the satellite era. *Environmental Research Letters*, 13(6): 063008, jun 2018. ISSN 1748-9326. URL `http://stacks.iop.org/1748-9326/13/i=6/a=063008?key=crossref.a29d19ff8e92d45a021c6aca08d2c874`.

Jonathan L. Bamber, Michael Oppenheimer, Robert E. Kopp, Willy P. Aspinall, and Roger M. Cooke. Ice sheet contributions to future sea-level rise from structured expert judgment. *Proceedings of the National Academy of Sciences*, 116(23):11195–11200, May 2019. doi: $10.1073/\text{pnas.}1817205116$. URL `https://doi.org/10.1073/pnas.1817205116`.

Per Berg and Jacob Weismann Poulsen. Implementation details for hbm. Technical Report 12-11, Danish Meteorological Institute, 2012. URL `https://www.dmi.dk/fileadmin/Rapporter/TR/tr12-11.pdf`.

John Cappelen. Ekstrem nedbør i danmark, opgørelser og analyser til og med 2016. Technical Report 17-06, Danish Meteorological Institute, 2017. URL `https://www.dmi.dk/fileadmin/user_upload/Rapporter/TR/2017/DMIRep17-06.pdf`.

John Cappelen. Ekstrem nedbør i danmark - opgørelser og analyser til og med 2018, tr19-06. Technical report, Danish Meteorological Institute, 2019. URL `https://www.dmi.dk/fileadmin/user_upload/Rapporter/TR/2019/DMIRap19-06.pdf`.

Bo Christiansen. Comparing cmip6 and cmip5: The road forward for the danish klimaatlas. Technical Report 22-38, Danish Meteorological Institute, 2022. URL `https://www.dmi.dk/fileadmin/Rapporter/2022/DMI_rapport_22-38.pdf`.

J. A. Church, P. U. Clark, A. Cazenave, J. M. Gregory, S. Jevrejeva, A. Levermann, M. A. Merrifield, G. A. Milne, R. S. Nerem, P. D. Nunn, A. J. Payne, W. T. Pfeffer, D. Stammer, and A. S. Unnikrishnan. Sea-level rise by 2100. *Science*, 342(6165):1445–1445, December 2013a. doi: 10.1126/science.342.6165.1445-a. URL `https://doi.org/10.1126/science.342.6165.1445-a`.

J.A. Church, P.U. Clark, A. Cazenave, J.M. Gregory, S. Jevrejeva, A. Levermann, M.A. Merrifield, G.A. Milne, R.S. Nerem, P.D. Nunn, A.J. Payne, W.T. Pfeffer, D. Stammer, and A.S. Unnikrishnan. *Sea Level Change*, book section 13, page 1137–1216. Cambridge University Press, Cambridge, United Kingdom and New York, NY, USA, 2013b. ISBN 978-1-107-66182-0. doi: 10.1017/CBO9781107415324.026. URL `www.climatechange2013.org`. *Editors: Stocker, T.F. and Qin, D. and Plattner, G.-K. and Tignor, M. and Allen, S.K. and Boschung, J. and Nauels, A. and Xia, Y. and Bex, V. and Midgley, P.M.*

Stuart Coles. *An Introduction to Statistical Modeling of Extreme Values*. Springer London, 2001. doi: https://doi.org/10.1007/978-1-4471-3675-0.

Sönke Dangendorf, Marta Marcos, Guy Wöppelmann, Clinton P. Conrad, Thomas Frederikse, and Riccardo Riva. Reassessment of 20th century global mean sea level rise. *Proceedings of the National Academy of Sciences*, 114(23):5946–5951, May 2017. doi: 10.1073/pnas.1616007114. URL `https://doi.org/10.1073/pnas.1616007114`.

Danmarks Statistik. Kvadratnet, 2019. URL `https://www.dst.dk/da/TilSalg/produkter/geodata/kvadratnet`.

Robert M. DeConto and David Pollard. Contribution of antarctica to past and future sea-level rise. *Nature*, 531(7596):591–597, March 2016. doi: 10.1038/nature17145. URL `https://doi.org/10.1038/nature17145`.

Charlotte Ditlevsen, Marta Ramos, Carlo Sørensen, Ulf Ciocan, and Thorsten Piontkowitz. Højvandsstatistikker 2017. Technical report, Kystdirektoratet, 2019. URL `https://kyst.dk/media/80372/hoejvandsstatistikker2017revideret11022019.pdf`.

M. G. Donat, G. C. Leckebusch, S. Wild, and U. Ulbrich. Future changes in european winter storm losses and extreme wind speeds inferred from GCM and RCM multi-model simulations. *Natural Hazards and Earth System Science*, 11(5):1351–1370, May 2011. doi: 10.5194/nhess-11-1351-2011. URL `https://doi.org/10.5194/nhess-11-1351-2011`.

Markus G Donat, Gregor C Leckebusch, Simon Wild, and Uwe Ulbrich. Benefits and limitations of regional multi-model ensembles for storm loss estimations. *Climate Research*, 44(2-3): 211–225, 2010. doi: 10.3354/cr00891. URL `https://doi.org/10.3354/cr00891`.

T Edwards, L Brandon, M A G Durand, and N R Edwards. Revisiting antarctic ice loss due to marine ice-cliff instability. *Nature*, 566(7742):58–64, 2019. doi: doi:10.1038/s41586-019-0901-4. URL `https://doi.org/10.1038/s41586-019-0901-4`.

B. Fox-Kemper, H.T. Hewitt, C. Xiao, G. Aðalgeirsdóttir, S.S. Drijfhout, T.L. Edwards, N.R. Golledge, M. Hemer, R.E. Kopp, G. Krinner, A. Mix, D. Notz, S. Nowicki, I.S. Nurhati, L. Ruiz, J.-B. Sallée, A.B.A. Slangen, and Y. Yu. Ocean, Cryosphere and Sea Level Change. In V. Masson-Delmotte, P. Zhai, A. Pirani, S. L. Connors, C. Péan, S. Berger, N. Caud, Y. Chen, L. Goldfarb, M. I. Gomis, M. Huang, K. Leitzell, E. Lonnoy, J. B. R. Matthews, T. K. Maycock, T. Waterfield, O. Yelekçi, R. Yu, and B. Zhou, editors, *Climate Change 2021: The Physical Science Basis. Contribution of Working Group I to the Sixth Assessment Report of the Intergovernmental Panel on Climate Change*, book section 4. Cambridge University Press, Cambridge, United Kingdom and New York, NY, USA, 2021. URL `https://www.ipcc.ch/report/ar6/wg1/downloads/report/IPCC_AR6_WGI_Chapter_09.pdf`.

W Fu, J She, and M Dobrynin. A 20-year reanalysis experiment in the Baltic Sea using three-dimensional variational (3DVAR) method. *Ocean Science*, 8(5):827–844, 2012. doi: $10.5194/os\text{-}8\text{-}827\text{-}2012$.

Gregory G Garner and Robert E Kopp. Framework for assessing changes to sea-level (FACTS) modules, scripts, and data for the IPCC AR6 sea level projections, 2022.

I. B. Gregersen, H. Madsen, J.J. Linde, Krüger, and K. Arnbjerg-Nielsen. Opdaterede klimafaktorer og dimensionsgivende regnintensiteter Skrift nr. 30. Technical report, Spildevandskomiteen, 2014a.

I. B. Gregersen, M. Sunyer, H. Madsen, S. Funder, J. Luchner, and D. Ros. Past, present, and future variations of extreme precipitation in denmark. Technical report, Danish Technical University, 2014b.

Lonny Hansen. Sea level data 1889-2017 from 14 stations in denmark mean, maximum and minimum values calculated on monthly and yearly basis including plots of mean values. Technical Report 18-16, Danish Meteorological Institute, 2018. URL `https://www.dmi.dk/fileadmin/Rapporter/2018/DMI_Report_18-16.pdf`.

Carling C Hay, Eric Morrow, Robert E Kopp, and Jerry X Mitrovica. Probabilistic reanalysis of twentieth-century sea-level rise. *Nature*, 517(7535):481, 2015. doi: $doi{:}10.1038/nature14093$.

Simon J. Holgate, Andrew Matthews, Philip L. Woodworth, Lesley J. Rickards, Mark E. Tamisiea, Elizabeth Bradshaw, Peter R. Foden, Kathleen M. Gordon, Svetlana Jevrejeva, and Jeff Pugh. New data systems and products at the permanent service for mean sea level. *Journal of Coastal Research*, pages 493–504, 2013. doi: $10.2112/JCOASTRES\text{-}D\text{-}12\text{-}00175.1$. URL `https://doi.org/10.2112/JCOASTRES-D-12-00175.1`.

J. R. M. Hosking, J. R. Wallis, and E. F. Wood. Estimation of the Generalized Extreme-Value Distribution by the Method of Probability-Weighted Moments. *Technometrics*, 27(3):251, August 1985. ISSN 00401706. URL `http://www.jstor.org/stable/1269706?origin=crossref`.

J. R.M. Hosking and J. R. Wallis. Parameter and quantile estimation for the generalized pareto distribution. *Technometrics*, 29(3):339–349, August 1987. URL `https://doi.org/10.1080/00401706.1987.10488243`.

Daniela Jacob, Juliane Petersen, Bastian Eggert, Antoinette Alias, Ole Bøssing Christensen, Laurens M. Bouwer, Alain Braun, Augustin Colette, Michel Déqué, Goran Georgievski, Elena Georgopoulou, Andreas Gobiet, Laurent Menut, Grigory Nikulin, Andreas Haensler, Nils Hempelmann, Colin Jones, Klaus Keuler, Sari Kovats, Nico Kröner, Sven Kotlarski, Arne Kriegsmann, Eric Martin, Erik van Meijgaard, Christopher Moseley, Susanne Pfeifer, Swantje Preuschmann, Christine Radermacher, Kai Radtke, Diana Rechid, Mark Rounsevell, Patrick Samuelsson, Samuel Somot, Jean Francois Soussana, Claas Teichmann, Riccardo Valentini, Robert Vautard, Björn Weber, and Pascal Yiou. EURO-CORDEX: New high-resolution climate change projections for European impact research. *Regional Environmental Change*, 14(2):563–578, 2014. doi: $10.1007/s10113-013-0499-2$.

A. F G Jacobs and H. A R De Bruin. Makkink's equation for evapotranspiration applied to unstressed maize. *Hydrological Processes*, 12:1063–1066, 1998. ISSN 08856087. doi: $10.1002/(SICI)1099-1085(19980615)12:7<1063::AID-HYP640>3.0.CO;2-2$.

Thomas Jacobsen, Carlo Sørensen, Jacob Woge Nielsen, and Jian Su. Dmi report 21-28, historical extreme high water levels along the coastline of denmark final scientific report of the 2020 national centre for climate research work package 2.2.3 ekstremhav. Technical Report 21-28, Danish Meteorological Institute, 2021. URL `https://www.dmi.dk/fileadmin/Rapporter/2021/DMI_Report_21-28.pdf`.

H. Madsen, I. B. Gregersen, D. Rosbjerg, and K. Arnbjerg-Nielsen. Regional frequency analysis of short duration rainfall extremes using gridded daily rainfall data as co-variate. *Water Science and Technology*, 75(8):1971–1981, February 2017. URL `https://doi.org/10.2166/wst.2017.089`.

Moritz Mathis, B Mayer, and Thomas Pohlmann. An uncoupled dynamical downscaling for the North Sea: method and evaluation. *Ocean Modelling*, 72:153–166, 2013. URL `https://doi.org/10.1016/j.ocemod.2013.09.004`.

Mathworks. The *scatteredInterpolant* routine, 2019. URL `https://se.mathworks.com/help/matlab/ref/scatteredinterpolant.html`.

Jerry X Mitrovica and Glenn A Milne. On post-glacial sea level: I. General theory. *Geophysical Journal International*, 154(2):253–267, 2003. URL `https://doi.org/10.1046/j.1365-246X.2003.01942.x`.

Jerry X Mitrovica, Natalya Gomez, and Peter U Clark. The sea-level fingerprint of West Antarctic collapse. *Science*, 323(5915):753–753, 2009. URL `https://science.sciencemag.org/content/323/5915/753`.

Jerry X Mitrovica, N Gomez, E Morrow, C Hay, K Latychev, and ME Tamisiea. On the robustness of predictions of sea level fingerprints. *Geophysical Journal International*, 187 (2):729–742, 2011. URL `https://doi.org/10.1111/j.1365-246X.2011.05090.x`.

MST. Miljøstyrelsen, 2019. URL `https://mst.dk`.

Sanne Muis, Martin Verlaan, Hessel C Winsemius, Jeroen CJH Aerts, and Philip J Ward. A global reanalysis of storm surges and extreme sea levels. *Nature communications*, 7:11969, 2016. URL `https://doi.org/10.1038/ncomms11969`.

Robert S Nerem, Brian D Beckley, John T Fasullo, Benjamin D Hamlington, Dallas Masters, and Gary T Mitchum. Climate-change–driven accelerated sea-level rise detected in the altimeter era. *Proceedings of the National Academy of Sciences*, 115(9):2022–2025, 2018. URL `https://doi.org/10.1073/pnas.1717312115`.

Martin Olesen, Kristine Skovgaard Madsen, Carsten Ankjær Ludwigsen, Fredrik Boberg, Tina Christensen, John Cappelen, Ole Bøssing Christensen, Katrine Krogh Andersen, and Jens Hesselbjerg Christensen. Fremtidige klimaforandringer i danmark. Technical Report 14-06, DMI, 2014. URL `https://www.dmi.dk/fileadmin/user_upload/Rapporter/DKC/2014/Klimaforandringer_dmi.pdf`.

M. Oppenheimer, Glavovic B., Hinkel J., R. van de Wal, A. Magen, A. Abd-Elgawad, R.S. Cai, M. Cifuentes-Jara, R.M. Deconto, T. Ghosh, J. Hay, F. Isla, B. Marzeion, B. Meyssignac, and Z. Sebesvari. *Sea Level Rise and Implications for Low Lying Islands, Coasts and Communities*, book 4. in press, 2019. URL `www.ipcc.ch/srocc/download-report`. Please be aware that this citation is the draft version, the final version will be available on the website after correction.

David T Pugh. *Tides, surges and mean sea level*. John Wiley and Sons Inc., New York, NY, 1987.

Madleine Samuelsson and Anders Stigebrandt. Main characteristics of the long-term sea level variability in the baltic sea. *Tellus A*, 48(5):672–683, 1996. doi: 10.1034/j.1600-0870.1996.t01-4-00006.x. URL `https://onlinelibrary.wiley.com/doi/abs/10.1034/j.1600-0870.1996.t01-4-00006.x`.

Mikael Scharling. Klimagrid - danmark nedbør, lufttemperatur og potentiel fordampning 20x20 & 40x40 km - metodebeskrivelse. Technical Report 99-12, Danish Meteorological Institute, 1999. URL `https://www.dmi.dk/fileadmin/user_upload/Rapporter/TR/1999/tr99-12.pdf`.

Mikael Scharling. Klimagrid Danmark nedbør 10x10 km (ver.2) - metodebeskrivelse. Technical Report 99-15, Danish Meteorological Institute, 2012. URL `https://www.dmi.dk/fileadmin/user_upload/Rapporter/TR/1999/tr99-15.pdf`.

Torben Schmith, Peter Thejll, Flemming Vejen, and Bo Christiansen. Regional variation of climatological cloudburst frequency estimated from historical observations of daily precipitation sums. *International Journal of Climatology*, 11 2023. ISSN 0899-8418. doi: $10.1002/\text{joc}.8291$.

SDFE. Styrelsen for dataforsyning og effektivisering, 2019. URL `https://sdfe.dk/hent-data/datafordeleren/`.

R Sibson. A brief description of natural neighbor interpolation. In V Barnett, editor, *Interpreting multivariate data*, pages 21–36. Wiley, Chichester, 1981.

Aimée BA Slangen, Benoit Meyssignac, Cecile Agosta, Nicolas Champollion, John A Church, Xavier Fettweis, Stefan RM Ligtenberg, Ben Marzeion, Angelique Melet, Matthew D Palmer, et al. Evaluating model simulations of twentieth-century sea level rise. Part I: global mean sea level change. *Journal of Climate*, 30(21):8539–8563, 2017. URL `https://doi.org/10.1175/JCLI-D-17-0110.1`.

Carlo Sørensen, H.T. Madsen, and S.B. Knudsen. Højvandsstatistikker 2012. Technical report, Kystdirektoratet, 2013.

Peter Riddersholm Wang and Mikael Scharling. Klimagrid danmark - dokumentation og validering af klimagrid danmark i 1x1 km opløsning. Technical Report 10-13, Danish Meteorological Institute, 2012. URL `https://www.dmi.dk/fileadmin/Rapporter/TR/tr10-13.pdf`.

Y Wang, K R Anderson, and R M Suddaby. Updated source code for calculating fire danger indices in the canadian forest fire weather index system. information report nor-x-424, 2015. ISSN 0831-8247.

Christopher S Watson, Neil J White, John A Church, Matt A King, Reed J Burgette, and Benoit Legresy. Unabated global mean sea-level rise over the satellite altimeter era. *Nature Climate Change*, 5(6):565–568, 2015. URL `https://www.nature.com/articles/nclimate2635`.

Philip L Woodworth, JR Hunter, Marta Marcos, P Caldwell, Margarita Menéndez, and I Haigh. Towards a global higher-frequency sea level dataset. *Geoscience Data Journal*, 3(2):50–59, 2016. URL `https://doi.org/10.1002/gdj3.42`.